



Identification of RipAZ1 as an avirulence determinant of *Ralstonia solanacearum* in *Solanum americanum*

Hayoung Moon¹ | Ankita Pandey¹ | Hayeon Yoon¹ | Sera Choi¹ | Hyelim Jeon^{2,3} | Maxim Prokchorchik¹ | Gayoung Jung¹ | Kamil Witek⁴ | Marc Valls ^{5,6} | Honour C. McCann^{7,8} | Min-Sung Kim^{1,9} | Jonathan D. G. Jones⁴ | Cécile Segonzac^{2,3,10} | Kee Hoon Sohn ^{1,11}

¹Department of Life Sciences, Pohang University of Science and Technology, Pohang, Republic of Korea

²Department of Agriculture, Forestry and Bioresources, Seoul National University, Seoul, Republic of Korea

³Plant Immunity Research Center, Seoul National University, Seoul, Republic of Korea

⁴The Sainsbury Laboratory, University of East Anglia, Norwich, UK

⁵Department of Genetics, University of Barcelona, Barcelona, Spain

⁶Centre for Research in Agricultural Genomics (CSIC-IRTA-UAB-UB), Bellaterra, Spain

⁷New Zealand Institute of Advanced Studies, Massey University, Auckland, New Zealand

⁸Max Planck Institute for Developmental Biology, Tübingen, Germany

⁹Division of Integrative Biosciences and Biotechnology, Pohang University of Science and Technology, Republic of Korea

¹⁰Department of Plant Science, Plant Genomics and Breeding Institute, Agricultural Life Science Research Institute, Seoul National University, Seoul, Republic of Korea

¹¹School of Interdisciplinary Bioscience and Bioengineering, Pohang University of Science and Technology, Pohang, Republic of Korea

Correspondence

Kee Hoon Sohn, Department of Life Sciences, Pohang University of Science and Technology, Pohang 37673, Republic of Korea.
Email: khsohn@postech.ac.kr

Funding information

National Research Foundation of Korea; Rural Development Administration, Grant/Award Number: PJ01317501; National Research Foundation, Grant/Award Number: PID2019-108595RB-I00, 2015 and 0533; Seoul National University; Generalitat de Catalunya

Abstract

Ralstonia solanacearum causes bacterial wilt disease in many plant species. Type III-secreted effectors (T3Es) play crucial roles in bacterial pathogenesis. However, some T3Es are recognized by corresponding disease resistance proteins and activate plant immunity. In this study, we identified the *R. solanacearum* T3E protein RipAZ1 (*Ralstonia* injected protein AZ1) as an avirulence determinant in the black nightshade species *Solanum americanum*. Based on the *S. americanum* accession-specific avirulence phenotype of *R. solanacearum* strain Pe_26, 12 candidate avirulence T3Es were selected for further analysis. Among these candidates, only RipAZ1 induced a cell death response when transiently expressed in a bacterial wilt-resistant *S. americanum* accession. Furthermore, loss of *ripAZ1* in the avirulent *R. solanacearum* strain Pe_26 resulted in acquired virulence. Our analysis of the natural sequence and functional variation of RipAZ1 demonstrated that the naturally occurring C-terminal truncation results in loss of RipAZ1-triggered cell death. We also show that the 213 amino acid central region of RipAZ1 is sufficient to induce cell death in *S. americanum*. Finally, we show that RipAZ1 may activate defence in host cell cytoplasm. Taken together, our data indicate that the nucleocytoplasmic T3E RipAZ1 confers *R. solanacearum*

This is an open access article under the terms of the Creative Commons Attribution-NonCommercial License, which permits use, distribution and reproduction in any medium, provided the original work is properly cited and is not used for commercial purposes.

© 2021 The Authors. *Molecular Plant Pathology* published by British Society for Plant Pathology and John Wiley & Sons Ltd

avirulence in *S. americanum*. Few avirulence genes are known in vascular bacterial phytopathogens and *ripAZ1* is the first one in *R. solanacearum* that is recognized in black nightshades. This work thus opens the way for the identification of disease resistance genes responsible for the specific recognition of RipAZ1, which can be a source of resistance against the devastating bacterial wilt disease.

KEYWORDS

avirulence, bacterial wilt, effector, effector-triggered immunity, *Ralstonia solanacearum*, *Solanum americanum*

1 | INTRODUCTION

Many bacterial pathogens translocate a suite of virulence proteins termed effectors into invading host cells via a type III secretion system to suppress plant defence responses such as the generation of reactive oxygen species (ROS) (Jwa & Hwang, 2017; Macho & Zipfel, 2015). However, some effectors are recognized by corresponding plant disease resistance (R) proteins that activate effector-triggered immunity (ETI), resulting in restriction of pathogen proliferation (Cesari, 2018; Jones et al., 2016). The effectors that are recognized by R proteins are termed avirulence (Avr) proteins. The intracellular R proteins often carry nucleotide-binding (NB) and leucine-rich repeat (LRR) domains (Jones & Dangl, 2006; Qi & Innes, 2013). The sequences of NB-LRR receptor (NLR) proteins are highly polymorphic, presumably due to a molecular arms race shaped by coevolution with their corresponding Avr proteins (Baggs et al., 2017; Bergelson et al., 2001). Consequently, significant natural variation for NLR-dependent Avr effector recognition is often observed within a plant species (Ma et al., 2006; McCann & Guttman, 2008).

Ralstonia solanacearum causes bacterial wilt that results in significant losses during crop cultivation. Bacterial wilt causes severe damage in more than 200 plant species, including many solanaceous crops such as tomato, potato, and pepper (Genin & Denny, 2012). *R. solanacearum* is a soilborne bacterium, entering host plant roots mostly through natural wounds, and colonizes plant xylem vessels, resulting in wilt symptoms (Denny, 2007). *R. solanacearum* is often referred to as the *Ralstonia solanacearum* species complex (RSSC) due to its extensive genetic diversity (Fegan & Prior, 2005). RSSC is classified into four phylotypes based on genomic sequence diversity that roughly correlate to geographical distribution: phylotype I to Asia, phylotype IIA and IIB to the Americas, phylotype III to Africa, and phylotype IV to Australia and Indonesia (Fegan & Prior, 2005).

R. solanacearum virulence requires type III secretion system effectors (T3Es) that are translocated into host plant cells during infection (Coll & Valls, 2013; Genin & Denny, 2012). Extensive genomic and transcriptomic studies have uncovered the T3E repertoires in the RSSC (Genin & Denny, 2012; Mukaihara et al., 2010; Occhialini et al., 2005; Peeters et al., 2013; Prokhorchik et al., 2020; Sabbagh et al., 2019; Valls et al., 2006). In addition, several T3Es from *R. solanacearum* have been reported to trigger disease resistance

in plants. For example, *Pseudomonas* outer protein P2 (PopP2, also known as RipP2) is an acetyltransferase that is recognized by the paired NLR proteins RPS4 (resistance to *Pseudomonas syringae* 4) and RRS1 (resistance to *Ralstonia solanacearum* 1) in *Arabidopsis thaliana* (Deslandes et al., 2003, 2003; Narusaka et al., 2009). On translocation in the plant cell nucleus, PopP2 acetylates the RRS1 WRKY DNA-binding domain, reconfigures RRS1, and activates RPS4-dependent immunity (Guo et al., 2020; Le Roux et al., 2015; Sarris et al., 2015). Another *R. solanacearum* effector, *Ralstonia* injected protein B (RipB), triggers Roq1 (Recognition of XopQ 1)-dependent disease resistance in *Nicotiana benthamiana* (Nakano & Mukaihara, 2019). Interestingly, Roq1 was originally identified to recognize *Pseudomonas* and *Xanthomonas* effectors HopQ1 and XopQ, respectively (Schultink et al., 2017). Importantly, transgenic expression of RPS4/RRS1 or Roq1 in tomato confers bacterial wilt resistance (Narusaka et al., 2013; Thomas et al., 2020). More recently, the *Solanum lycopersicoides* NLR protein Ptr1 was shown to recognize RipBN and *P. syringae* effector AvrRpt2 (Mazo-Molina et al., 2019). In addition to these avirulence effectors for which corresponding NLRs have been identified, the *R. solanacearum* effectors AvrA (RipAA) and RipAX2 act as avirulence proteins that induce bacterial wilt resistance in tobacco and eggplant, respectively (Morel et al., 2018; Poueymiro et al., 2009). PopP1 (RipP1) plays a role in avirulence in tobacco and petunia (Chen et al., 2018; Lavie et al., 2002; Poueymiro et al., 2009). Moreover, several *R. solanacearum* effectors were shown to induce cell death when transiently expressed in plant cells, such as AWR1 (RipA1) (Jeon et al., 2020; Prokhorchik et al., 2020; Sole et al., 2012), AWR2 (RipA2), AWR4 (RipA4), AWR5 (RipA5) (Sole et al., 2012), RipE1 (Jeon et al., 2020; Prokhorchik et al., 2020; Sang et al., 2020), RipI (Zhuo et al., 2020), PopA (RipX) (Arlat et al., 1994; Belbahri et al., 2001; Racape et al., 2005), RipAB (Zheng et al., 2019), RipAT, RipAV (Clarke et al., 2015; Wroblewski et al., 2009) and RipTPS (Poueymiro et al., 2014).

Black nightshades such as *Solanum americanum* and *Solanum nigrum* are herbaceous plants with a worldwide distribution that are thought to have great genetic diversity (Edmonds & Chweya, 1997; Sarkinen et al., 2018). Several studies have shown that black nightshades are a useful, underexploited source of disease resistance. For instance, *S. nigrum* is resistant to tobacco mosaic virus, potato late blight, and *Phomopsis* fruit rot (Edmonds & Chweya, 1997). The potato

late blight resistance gene *Rpi-amr3* (Resistance to *Phytophthora infestans*) was identified in *S. americanum*, a possible diploid ancestor of *S. nigrum* (Ganapathi & Rao, 1987; Witek et al., 2016).

Identification of a novel avirulence protein is an important step to develop disease resistance. As black nightshades can be a source of *R* genes for other pathogens (Edmonds & Chweya, 1997; Witek et al., 2016), we hypothesized that some black nightshade accessions might harbour bacterial wilt resistance genes. In this study, we identified *R. solanacearum* T3E RipAZ1 as an avirulence determinant in *S. americanum* using a bacterial wilt disease assay and comparative genomics analysis. We showed that the deletion of *ripAZ1* in an avirulent *R. solanacearum* strain resulted in bacterial wilt disease symptom development in a resistant *S. americanum* accession. We show that cytoplasmic localization may be required for RipAZ1-induced cell death in *S. americanum*.

2 | RESULTS

2.1 | *S. americanum* shows accession-specific bacterial wilt resistance

To identify a bacterial wilt resistance source in black nightshades, we tested 26 *S. americanum* accessions (Table S1) for disease susceptibility to seven *R. solanacearum* phylotype I strains isolated from diseased pepper (Pe_1, Pe_13, Pe_26, Pe_57) or tomato (To_1, To_7, To_63) plants in Korea (Table 1) (Segonzac et al., 2017). *S. americanum* plants were infected with *R. solanacearum* using the soil-drenching method and wilt symptoms were observed at 14 days postinfection (dpi). Among these interactions, we found that *R. solanacearum* strains Pe_26 and To_1 showed the most reproducible and robust avirulence and virulence phenotypes, respectively, in *S. americanum* accession SP2273. Therefore, these two strains were chosen for further analysis. *R. solanacearum* Pe_26 caused strong disease symptoms in *S. americanum* SP2275 but not in SP2273 (Figure 1a). In contrast, *R. solanacearum* To_1 caused comparable disease symptoms in both accessions SP2273 and SP2275 (Figure 1a). In addition, we performed a quantitative assessment of disease by calculating the survival rate of the *S. americanum* plants infected with *R. solanacearum* Pe_26 or To_1 (Figure 1b). Only the *S. americanum* SP2273 plants infected with *R. solanacearum* Pe_26 showed a significantly high survival rate at 10 dpi (Figure 1b). These data suggest that *R. solanacearum* Pe_26 may carry an avirulence effector(s) that triggers bacterial wilt disease resistance in *S. americanum* SP2273.

2.2 | *R. solanacearum* effector RipAZ1 induces accession-specific cell death in *S. americanum*

We hypothesized that an avirulence effector is present in Pe_26 but absent or showing significant sequence polymorphism in To_1. Recently, the genome sequences and T3E repertoires of multiple *R. solanacearum* phylotype I strains, including Pe_26 and To_1, were

reported (Prokhorchik et al., 2020). To identify the candidate avirulence effectors, effector repertoires of Pe_26 and To_1 strains were compared with the following criteria. First, the five T3Es, RipBA, RipG1, RipTAL, RipY, and RS_T3E_Hyp6, which are present in the avirulent strain Pe_26 but absent in the virulent To_1, were selected. Second, the seven T3Es, RipAX1, RipG6, RipAZ1, AWR3 (RipA3), RipB, RipD, and RipJ, which are present in both strains but showing less than 95% amino acid identity, were chosen. As a result, a total of 12 candidate avirulence effectors were selected.

Pathogen avirulence proteins often induce cell death when transiently expressed in plant cells using *Agrobacterium*-mediated transient transformation (hereafter, agroinfiltration). To identify the avirulence effector that induces cell death in *S. americanum* SP2273 but not SP2275, the 12 selected candidate avirulence effector genes were cloned with a C-terminal FLAG tag under the control of the constitutive cauliflower mosaic virus (CaMV) 35S promoter. The *R. solanacearum* GMI1000 allele of the effector RipA1 with the C-terminal FLAG tag was used as a positive control because it induced robust cell death in all tested *S. americanum* accessions (data not shown), including SP2273 and SP2275, when transiently expressed (Figures 2a and S1), as well as in *N. benthamiana* (Jeon et al., 2020; Prokhorchik et al., 2020; Sole et al., 2012). C-terminal FLAG-tagged yellow fluorescent protein (YFP) was expressed as a negative control. Agroinfiltration of each of the 12 candidate avirulence effectors in *S. americanum* SP2275 did not result in cell death, in contrast to RipA1_{GMI1000} (Figure S1). However, agroinfiltration of the candidate avirulence effector RipAZ1 induced strong cell death in SP2273 (Figure 2a). Next, we quantified the RipAZ1-induced *S. americanum* accession-specific cell death using an electrolyte leakage assay (Figure 2b). As expected, RipA1_{GMI1000} induced a robust increase in conductivity in SP2273 and SP2275 while YFP did not (Figure 2b). Consistent with our cell death assay results (Figure 2a), agroinfiltration of RipAZ1 led to increased conductivity, comparable to RipA1_{GMI1000} in *S. americanum* SP2273 but not in SP2275 (Figure 2b). This result further demonstrates that RipAZ1-triggered cell death in *S. americanum* is accession-specific. The lack of RipAZ1-induced cell death in SP2275 was not due to protein instability because transiently expressed RipAZ1-FLAG protein was stable (Figure S2). Our data therefore strongly suggest that RipAZ1 may function as a major avirulence determinant in SP2273. However, we cannot exclude the possibility that RipTAL, RipY, and RipA3 may have not induced cell death due to the lack of protein expression (Figure S2).

2.3 | RipAZ1 confers *R. solanacearum* avirulence in *S. americanum* SP2273

We next hypothesized that a loss of function mutation in *ripAZ1* would enable *R. solanacearum* Pe_26 to cause disease in the resistant *S. americanum* accession SP2273. A *ripAZ1* knockout mutant was constructed by replacing the *ripAZ1* open reading frame (ORF) with a spectinomycin resistance (*Spec^R*) cassette through homologous recombination using pRCgg- Δ *ripAZ1* (Table 1, and Figures S3a and S4a). The resulting *R. solanacearum* Pe_26 Δ *ripAZ1* mutant

TABLE 1 Bacterial strains and plasmids used in this study

Strain or plasmid	Relevant characteristics	Source or reference
Strains		
<i>Ralstonia solanacearum</i>		
Pe_1	Wild-type; isolated from a diseased commercial pepper plant in Korea	Segonzac et al. (2017)
Pe_13	Wild-type; isolated from a diseased commercial pepper plant in Korea	Segonzac et al. (2017)
Pe_26	Wild-type; isolated from a diseased commercial pepper plant in Korea	Segonzac et al. (2017)
Pe_26 Δ ripAZ1	In-frame deletion of <i>ripAZ1</i> replaced by spectinomycin resistance (Spec ^R) cassette using pRCgg- Δ ripAZ1; Spec ^R	This study
Pe_26 Δ ripAZ1 (<i>ripAZ1</i>)	<i>ripAZ1</i> complementation in Pe_26 Δ ripAZ1 using pRCKgg- <i>PhB-ripAZ1-FLAG</i> ; Spec ^R , kanamycin resistance (Kan ^R)	This study
Pe_57	Wild-type; isolated from a diseased commercial pepper plant in Korea	Segonzac et al. (2017)
To_1	Wild-type; isolated from a diseased commercial tomato plant in Korea	Segonzac et al. (2017)
To_7	Wild-type; isolated from a diseased commercial tomato plant in Korea	Segonzac et al. (2017)
To_63	Wild-type; isolated from a diseased commercial tomato plant in Korea	Segonzac et al. (2017)
<i>Escherichia coli</i>		
DH5 α	Wild-type	Laboratory collection
<i>Agrobacterium tumefaciens</i>		
AGL1	Wild-type; ampicillin resistance (Amp ^R)	Laboratory collection
Plasmids		
pICH41021	Modified pUC19 vector in which the internal <i>Bsa</i> I recognition site is mutated; Amp ^R	Laboratory collection
pICH86988	Binary vector carrying CaMV 35S promoter; Kan ^R	Weber et al. (2011)
pICH86988- <i>ripA1</i> _{GMI1000} -FLAG	<i>ripA1</i> _{GMI1000} -FLAG cloned in pICH86988; Kan ^R	Laboratory collection
pICH86988-YFP-FLAG	YFP-FLAG cloned in pICH86988; Kan ^R	Laboratory collection
pICH86988-FLAG-GFP	FLAG-GFP cloned in pICH86988; Kan ^R	Laboratory collection
pICH86988- <i>ripAZ1</i> _{Pe_26} -FLAG	<i>ripAZ1</i> _{Pe_26} -FLAG cloned in pICH86988; Kan ^R	This study
pICH86988- <i>ripTAL</i> -FLAG	<i>ripTAL</i> -FLAG cloned in pICH86988; Kan ^R	This study
pICH86988- <i>ripY</i> -FLAG	<i>ripY</i> -FLAG cloned in pICH86988; Kan ^R	This study
pICH86988- <i>RS_T3E_Hyp6</i> -FLAG	<i>RS_T3E_Hyp6</i> -FLAG cloned in pICH86988; Kan ^R	This study
pICH86988- <i>ripBA</i> -FLAG	<i>ripBA</i> -FLAG cloned in pICH86988; Kan ^R	This study
pICH86988- <i>ripG1</i> -FLAG	<i>ripG1</i> -FLAG cloned in pICH86988; Kan ^R	This study
pICH86988- <i>ripAX1</i> -FLAG	<i>ripAX1</i> -FLAG cloned in pICH86988; Kan ^R	This study
pICH86988- <i>ripB</i> -FLAG	<i>ripB1</i> -FLAG cloned in pICH86988; Kan ^R	This study
pICH86988- <i>ripG6</i> -FLAG	<i>ripG6</i> -FLAG cloned in pICH86988; Kan ^R	This study
pICH86988- <i>ripA3</i> -FLAG	<i>ripA3</i> -FLAG cloned in pICH86988; Kan ^R	This study
pICH86988- <i>ripD</i> -FLAG	<i>ripD</i> -FLAG cloned in pICH86988; Kan ^R	This study
pICH86988- <i>ripJ</i> -FLAG	<i>ripJ</i> -FLAG cloned in pICH86988; Kan ^R	This study
pICH86988- <i>ripAZ1</i> _{Pe_51} -FLAG	<i>ripAZ1</i> _{Pe_51} -FLAG cloned in pICH86988; Kan ^R	This study
pICH86988- <i>ripAZ1</i> _{Pe_57} -FLAG	<i>ripAZ1</i> _{Pe_57} -FLAG cloned in pICH86988; Kan ^R	This study
pICH86988- <i>ripAZ1</i> _{To_1} -FLAG	<i>ripAZ1</i> _{To_1} -FLAG cloned in pICH86988; Kan ^R	This study
pICH86988- <i>ripAZ1</i> _{SL3022} -FLAG	<i>ripAZ1</i> _{SL3022} -FLAG cloned in pICH86988; Kan ^R	This study
pICH86988- <i>ripAZ1</i> _{KACC10722} -FLAG	<i>ripAZ1</i> _{KACC10722} -FLAG cloned in pICH86988; Kan ^R	This study
pICH86988- <i>ripAZ1</i> ²⁴⁻²⁷⁷ -FLAG	<i>ripAZ1</i> ²⁴⁻²⁷⁷ -FLAG cloned in pICH86988; Kan ^R	This study
pICH86988- <i>ripAZ1</i> ⁵⁹⁻²⁷⁷ -FLAG	<i>ripAZ1</i> ⁵⁹⁻²⁷⁷ -FLAG cloned in pICH86988; Kan ^R	This study
pICH86988- <i>ripAZ1</i> ⁸⁷⁻²⁷⁷ -FLAG	<i>ripAZ1</i> ⁸⁷⁻²⁷⁷ -FLAG cloned in pICH86988; Kan ^R	This study
pICH86988- <i>ripAZ1</i> ¹⁻²⁷¹ -FLAG	<i>ripAZ1</i> ¹⁻²⁷¹ -FLAG cloned in pICH86988; Kan ^R	This study

(Continues)

TABLE 1 (Continued)

Strain or plasmid	Relevant characteristics	Source or reference
pICH86988- <i>ripAZ1</i> ¹⁻²⁵⁵ -FLAG	<i>ripAZ1</i> ¹⁻²⁵⁵ -FLAG cloned in pICH86988; Kan ^R	This study
pICH86988- <i>ripAZ1</i> ⁵⁹⁻²⁷¹ -FLAG	<i>ripAZ1</i> ⁵⁹⁻²⁷¹ -FLAG cloned in pICH86988; Kan ^R	This study
pICH86988- <i>ripAZ1</i> _{To_1} -YFP	<i>ripAZ1</i> _{To_1} -YFP cloned in pICH86988; Kan ^R	This study
pICH86988- <i>ripAZ1</i> _{Pe_51} -YFP	<i>ripAZ1</i> _{Pe_51} -YFP cloned in pICH86988; Kan ^R	This study
pICH86988- <i>ripAZ1</i> _{Pe_51} -YFP-NES	<i>ripAZ1</i> _{Pe_51} -YFP-NES cloned in pICH86988; Kan ^R	This study
pICH86988- <i>ripAZ1</i> _{Pe_51} -YFP-NLS	<i>ripAZ1</i> _{Pe_51} -YFP-NLS cloned in pICH86988; Kan ^R	This study
pICH86988- <i>ripAZ1</i> _{Pe_51} -YFP-NES ^{mut}	<i>ripAZ1</i> _{Pe_51} -YFP-NES ^{mut} cloned in pICH86988; Kan ^R	This study
pICH86988- <i>ripAZ1</i> _{Pe_51} -YFP-NLS ^{mut}	<i>ripAZ1</i> _{Pe_51} -YFP-NLS ^{mut} cloned in pICH86988; Kan ^R	This study
pICH86988- <i>ripAZ1</i> _{Pe_26} -YFP	<i>ripAZ1</i> _{Pe_26} -YFP cloned in pICH86988; Kan ^R	This study
pRCgg	5'- <i>Bam</i> HI- <i>Bsa</i> I- <i>lacZ</i> - <i>Bsa</i> I- <i>Eco</i> RI-3' fragment cloned in pICH41021; Amp ^R	This study
pRCKgg	Modified pRCK vector (Monteiro et al., 2012) in which Gateway cassette is replaced with Golden Gate cassette (<i>lacZ</i>); Amp ^R , Kan ^R	This study
pRCgg- Δ <i>ripAZ1</i>	Spec ^R cassette from pCR8, flanked by 5' and 3' sequences of <i>ripAZ1</i> _{Pe_26} ORF, cloned in pRCgg; Amp ^R , Spec ^R	This study
pRCKgg- <i>PhB</i> - <i>ripAZ1</i> -FLAG	<i>ripAZ1</i> _{Pe_26} -FLAG under the control of <i>hrpB</i> promoter (<i>PhB</i>) cloned in pRCKgg; Amp ^R , Kan ^R	This study

strain was experimentally validated to carry the desired mutation (Figure S4b). To test if RipAZ1 is required for *R. solanacearum* Pe_26 avirulence, the resistant and susceptible *S. americanum* accessions were infected with wild-type or Δ *ripAZ1* mutant Pe_26 strain using the soil-drenching infection assay. As expected, wild-type *R. solanacearum* Pe_26 caused severe wilt symptoms in *S. americanum* SP2275, whereas SP2273 remained healthy (Figure 3a). In contrast, *R. solanacearum* Pe_26 Δ *ripAZ1* caused comparable wilt symptoms in both *S. americanum* accessions (Figure 3a). Importantly, the complemented strain Pe_26 Δ *ripAZ1* carrying *ripAZ1*, constructed using pRCKgg-*PhB*-*ripAZ1*-FLAG (Table 1, and Figures S3b and S5), showed *S. americanum* SP2273-specific avirulence, demonstrating that RipAZ1 is the avirulence determinant (Figure 3a). We further assessed the survival rate of *S. americanum* plants infected with wild-type, Δ *ripAZ1*, or Δ *ripAZ1* (*ripAZ1*) strains of *R. solanacearum* Pe_26 (Figure 3b). None of the *S. americanum* SP2275 plants infected by Pe_26 Δ *ripAZ1* mutant strain survived at 10 dpi, suggesting that the loss of *ripAZ1* does not result in a significant decrease in virulence of *R. solanacearum* Pe_26 in the susceptible host plants (Figure 3b). In contrast, the *S. americanum* SP2273 plants showed a significantly higher survival rate when infected with *R. solanacearum* Pe_26 wild-type or Δ *ripAZ1* (*ripAZ1*) strain as compared to To_1 or Pe_26 Δ *ripAZ1* strain (Figure 3b). These results demonstrate that RipAZ1 confers *R. solanacearum* Pe_26 avirulence in *S. americanum*.

2.4 | The C-terminally truncated RipAZ1 natural variant is unable to induce cell death in *S. americanum*

Naturally occurring avirulence effectors often show significant sequence polymorphism in pathogen populations (Asai et al., 2018; Dodds et al., 2006). To survey natural sequence polymorphisms

of RipAZ1, we used the publicly available database RalstoT3E (<https://iant.toulouse.inra.fr/T3E> from Peeters et al., 2013) and the *R. solanacearum* phylotype I strain database from Prokhorchik et al. (2020) to identify 21 nonredundant RipAZ1 natural sequence variants (Table S2 and Figure S6). Phylogenetic analysis indicated that the RipAZ1 amino acid sequence of *R. solanacearum* phylotype IV strain SL3022 is the most distantly related to RipAZ1_{Pe_26} (Figure S6). Sequences of RipAZ1 natural variants from the same phylotype showed more than 80% amino acid sequence identity (Figures 4a and S7). The C-terminal region of pathogen effectors is often critical for function (Bos et al., 2006; Catanzariti et al., 2010; Yang et al., 2005; Yang & White, 2004). Interestingly, *ripAZ1*_{To_1} carries a one nucleotide base pair (bp) insertion that causes a frameshift and C-terminal truncation of 22 amino acids (Figures 4a and S7). In addition, RipAZ1 variants of phylotype IV strains carry 6-amino acid extended C-termini. Therefore, four representative phylotype I and two of the most distantly related phylotype IV variants were selected for further analysis (Figures 4a and S6). To compare the avirulence of RipAZ1 natural variants, we used an agroinfiltration assay in the resistant *S. americanum* accession SP2273. As previously shown, agroinfiltration of RipA1_{GMI1000} or the RipAZ1_{Pe_26} induced strong cell death, whereas YFP did not (Figure 4b). Importantly, agroinfiltration of RipAZ1 natural variants except RipAZ1_{To_1} induced strong cell death and high conductivity in *S. americanum* SP2273 (Figures 4b and S8, and Table S3). We found that RipAZ1_{To_1} protein accumulated to a similar level to other variants, indicating that the lack of cell death of RipAZ1_{To_1} is not due to protein instability (Figure 4c). These data indicate that RipAZ1 avirulence is conserved across different phylotypes and that the C-terminal region is indispensable for recognition.

Because RipAZ1 cannot induce cell death in *N. benthamiana*, we set out an experiment to test its ability to interfere with plant defence responses. We examined the amplitude of reactive oxygen species (ROS)

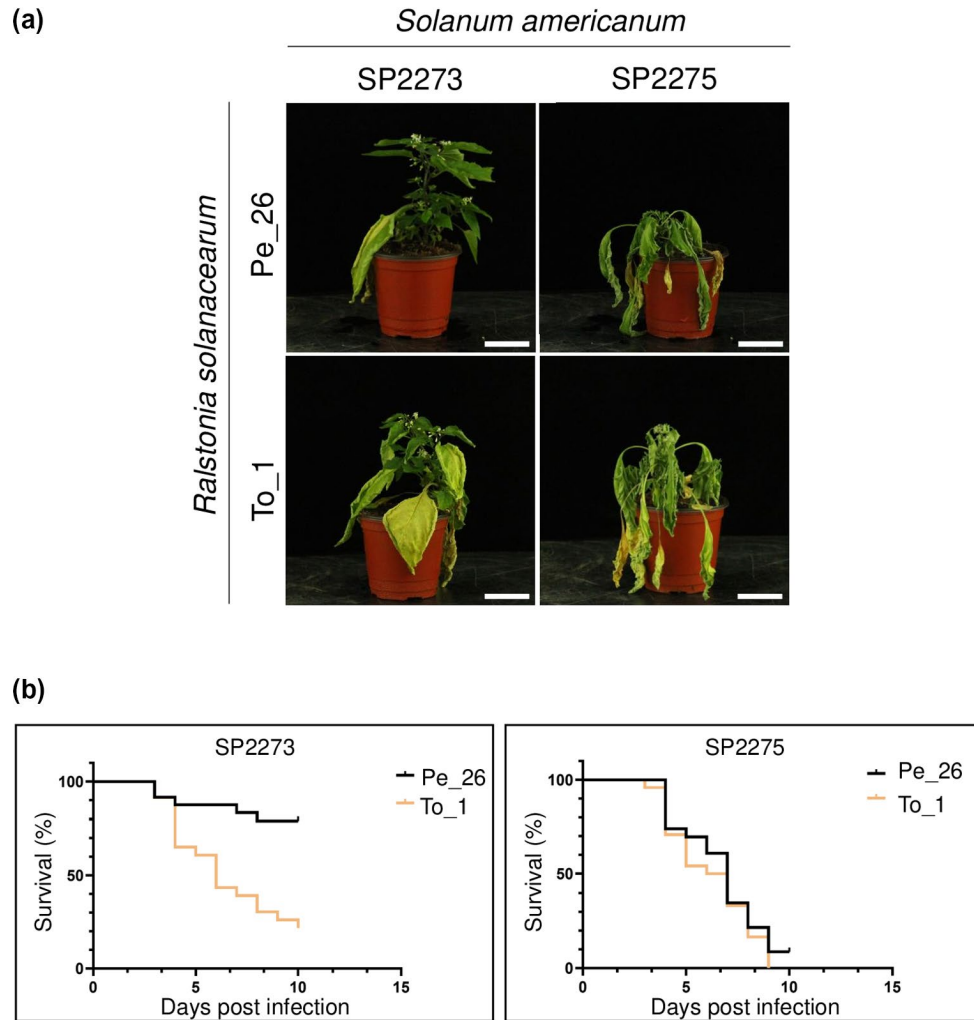


FIGURE 1 *Ralstonia solanacearum* strain Pe_26 induces accession-specific disease resistance in *Solanum americanum*. Bacterial wilt symptoms (a) and a survival graph (b) of the *S. americanum* accessions SP2273 and SP2275 infected with wild-type *R. solanacearum* strains Pe_26 and To_1. (a) Photographs from representative plants were taken at 14 days postinoculation. Scale bar = 5 cm. (b) The percentage of surviving plants was recorded for 10 days. The data used for the survival graph were collected from three independent experiments. Log-rank (Mantel-Cox) test *p* values are .0001 and .373 in SP2273 and SP2275, respectively

production and defence gene expression triggered by bacterial flagellin peptide flg22 in *N. benthamiana* leaves expressing YFP, RipAZ1_{Pe_26}, or RipAZ1_{To_1} (Figure S9). We observed a significant reduction of the total flg22-induced ROS production in the presence of RipAZ1_{Pe_26} but not of RipAZ1_{To_1} compared to the sample expressing YFP (Figure S9a). Similarly, the induction of NbACRE31 expression by flg22 was significantly reduced in leaves expressing RipAZ1_{Pe_26} compared to RipAZ1_{To_1} or YFP (Figure S9b). As both RipAZ1 variants accumulated to a similar level in *N. benthamiana* cells (Figure S9c), these data indicate that RipAZ1 could modulate the host defence responses and that the RipAZ1 C-terminal region might contribute to this function.

To survey the distribution of RipAZ1 in RSSC, we collected RipAZ1 sequence information from publicly available databases (Peeters et al., 2013; Prokhorchik et al., 2020). RipAZ1 was distributed in all four phylotypes among the 168 RSSC strains surveyed. Because *R. solanacearum* RipAZ1_{To_1} was the only experimentally validated virulent variant, we focused on identifying C-terminally

truncated natural variants and presence/absence polymorphism. RipAZ1 variants with C-terminal truncation were identified in only 33 *R. solanacearum* phylotype I strains (Table S2). Eighty strains across phylotypes carried full-length (255 amino acids) or C-terminally extended (284 amino acids) variants of the RipAZ1 sequence (Table S2). Interestingly, the C-terminally extended RipAZ1 sequence was found in much higher frequency in phylotype IV strains (23 out of 27 surveyed) compared to other phylotypes. These data further support a critical role for the C-terminal region of RipAZ1.

2.5 | The truncated variant RipAZ1⁵⁹⁻²⁷¹ induces cell death in *S. americanum*

To determine the minimal region required for RipAZ1 function, five N- or C-terminally truncated RipAZ1_{Pe_51} variants were generated based on the predicted secondary structure of the protein (Figures 5a and S10).

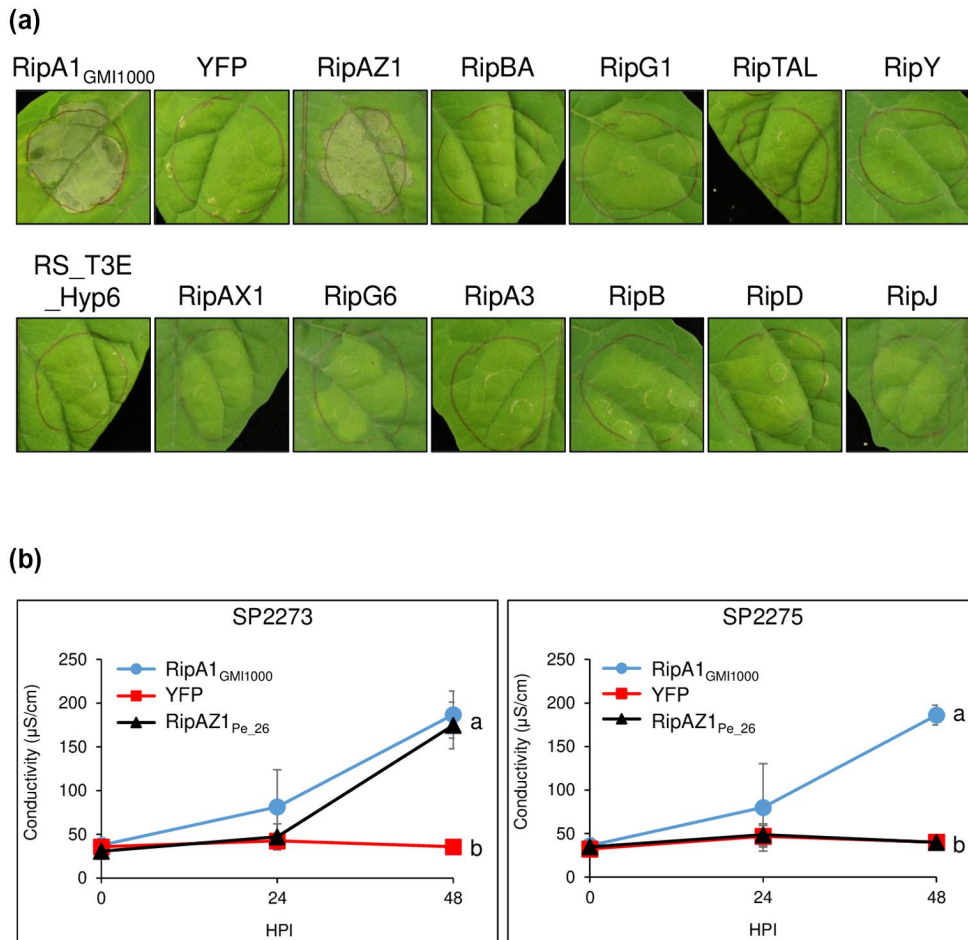


FIGURE 2 Overexpression of RipAZ1 induces cell death in *Solanum americanum* SP2273. (a) The candidate avirulence effectors were agroinfiltrated in SP2273 leaf epidermal cells. RipA1_{GMI1000} and yellow fluorescent protein (YFP) were used as controls. Photographs were taken at 2 days postinfiltration. White circles indicate the infected leaf area showing cell death. (b) Conductivity measurement of RipAZ1_{Pe_26} in SP2273 and SP2275. Four-week-old *S. americanum* leaves transiently expressing RipAZ1_{Pe_26} or control proteins, RipA1_{GMI1000} and YFP, using agroinfiltration were taken for conductivity measurements. HPI indicates hours postinfiltration. The data used were collected from three independent experiments. Coloured shapes and grey lines indicate means and standard deviations, respectively. Different letters indicate groups showing statistically significant differences at 48 HPI ($p < .05$; Student's *t* test). *p* values of circle–triangle, triangle–square, and square–circle are as follows: 0.343, 6.88×10^{-11} , and 2.33×10^{-11} in SP2273; 2.20×10^{-16} , 0.885, and 4.20×10^{-16} in SP2275

Agroinfiltration of the truncated RipAZ1_{Pe_51} variants did not lead to cell death in *S. americanum* SP2273 when N-terminal 86 (87–277) or C-terminal 22 (1–255) amino acids were absent (Figures 5b and S11, and Table S3). However, the loss of 58 N-terminal amino acids (59–277) or six C-terminal amino acids (1–271) did not affect RipAZ1-induced cell death (Figures 5b and S11, and Table S3). We next tested the RipAZ1^{59–271} variant in which 58 N-terminal and six C-terminal amino acids are truncated. Agroinfiltration of RipAZ1^{59–271} induced strong cell death that was comparable to that induced by full-length RipAZ1 (1–277) (Figures 5b and S11). Immunoblot analysis showed that all RipAZ1 variants were expressed, indicating that the loss of cell death-inducing activity in some truncated RipAZ1 variants was not due to protein instability (Figure 5c). Our results demonstrate that the centrally located region containing 213 amino acids is sufficient for RipAZ1 avirulence and that the predicted α -helices B and G (Figure S10) may be required for the avirulence.

2.6 | RipAZ1-YFP localizes in the nucleus and cytoplasm when transiently expressed in *N. benthamiana* leaf epidermal cells

To examine RipAZ1 localization in plant cells, C-terminally YFP-tagged RipAZ1 variants were transiently expressed in *N. benthamiana*. Agroinfiltration of RipAZ1-YFP triggered cell death comparable to RipAZ1-FLAG in *S. americanum* SP2273, indicating that RipAZ1-YFP is functional (Figure S12). RipAZ1_{Pe_26}-YFP and RipAZ1_{Pe_51}-YFP, which induce cell death in SP2273, were both localized in the nucleus and cytoplasm of *N. benthamiana* leaf epidermal cells (Figure S13). Similarly, RipAZ1_{To_1}-YFP, which does not trigger cell death in SP2273, also localized in the nucleus and cytoplasm when expressed in *N. benthamiana* leaves (Figure 6a). To investigate the contribution of RipAZ1 localization to its avirulence, we generated RipAZ1_{Pe_51}-YFP variants that are translationally fused to a nuclear

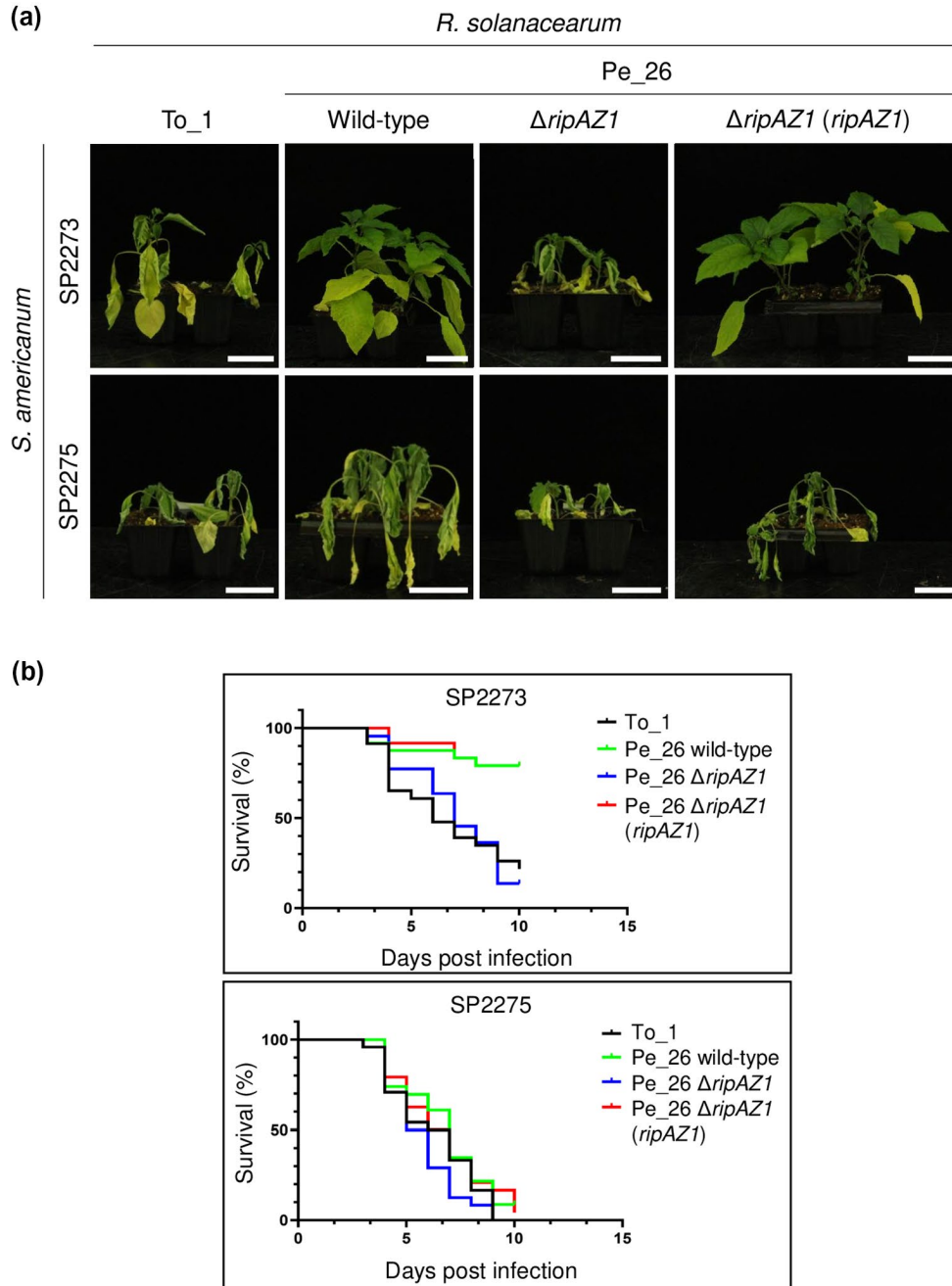


FIGURE 3 RipAZ1 triggers accession-specific immune responses in *Solanum americanum*. Bacterial wilt symptoms (a) and a survival graph (b) of accessions SP2273 and SP2275 infected with wild-type, $\Delta ripAZ1$, or $\Delta ripAZ1$ (*ripAZ1*) strain of Pe_26. (a) Photographs from representative plants were taken at 10 days postinfiltration. Scale bar = 5 cm. (b) The percentage of survival plants was recorded for 10–20 days. The data used for survival graphs were collected from three independent experiments. Log-rank (Mantel-Cox) test *p* values are <.0001 and .128 in SP2273 and SP2275, respectively

export signal (NES) or nuclear localization signal (NLS) (Heidrich et al., 2011; Wen et al., 1995). Nonfunctional variants of NES and NLS, NES^{mut} and NLS^{mut}, respectively, were used as controls. An immunoblot assay using anti-GFP antibody confirmed the stable expression of all RipAZ1-YFP variants in *N. benthamiana* leaf cells (Figure S14). RipAZ1_{Pe_51}-YFP-NES or RipAZ1_{Pe_51}-YFP-NLS mainly localized to the cytoplasm or nucleus, respectively (Figure 6a). As expected, RipAZ1_{Pe_51}-YFP-NES^{mut} and RipAZ1_{Pe_51}-YFP-NLS^{mut}

still showed the nucleocytoplasmic localization (Figure 6a). Next, we agroinfiltrated the RipAZ1-YFP variants in *S. americanum* SP2273 to test their cell death-inducing activity. Surprisingly, both RipAZ1_{Pe_51}-YFP-NES and RipAZ1_{Pe_51}-YFP-NLS variants induced cell death comparable to RipAZ1_{Pe_51}-YFP (Figures 6b and S15, and Table S3). However, we favour the hypothesis that RipAZ1 recognition occurs in the cytoplasm because RipAZ1_{Pe_51}-YFP-NLS could still induce defence responses prior to localization in the nucleus.

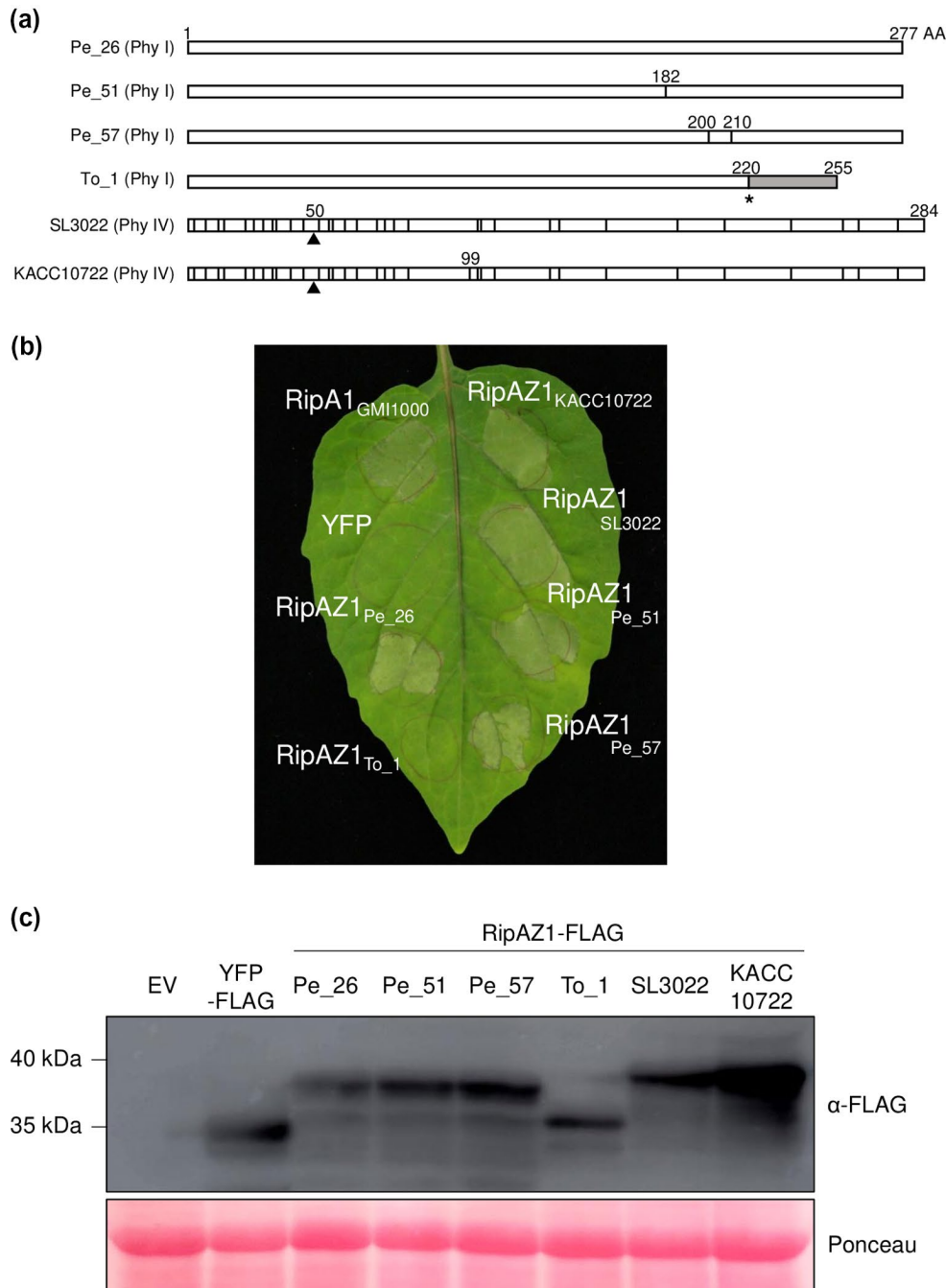


FIGURE 4 A naturally occurring C-terminally truncated RipAZ1 variant does not induce cell death in *Solanum americanum*. Amino acid sequence comparison (a), cell death responses in SP2273 (b), and western blot analysis in *Nicotiana benthamiana* (c) of the six representative RipAZ1 natural variants selected for functional analysis. (a) Nonsynonymous single nucleotide polymorphisms are indicated as black lines. A grey box indicates the region with no sequence identity due to a frameshift mutation caused by 1-base pair insertion as indicated with an asterisk. An amino acid in-frame-insertion is indicated with black triangles. Phylotype is abbreviated as “Phy”. (b) The photograph was taken at 2 days postinfiltration. White circles indicate the infected leaf area showing cell death. (c) Empty vector (EV; pICH86988) and yellow fluorescent protein (YFP)-FLAG were used as controls. Proteins were immunoblotted with anti-FLAG antibody. Leaf tissue was harvested at 2 days postinfiltration. Ponceau staining shows equal loading of proteins

3 | DISCUSSION

We show here that the effector RipAZ1 from the bacterial wilt-causing pathogen *R. solanacearum* triggers immunity in the wild Solanaceae species *S. americanum* SP2273. The *S. americanum*

accession-specific avirulence of *R. solanacearum* Pe_26 indicates that RipAZ1-induced cell death is more likely to be an ETI response than due to effector toxicity. Moreover, we identified the minimal region of RipAZ1 protein as RipAZ1⁵⁹⁻²⁷¹ that is sufficient to activate defence. Based on this result, RipAZ1 N-terminus, including a

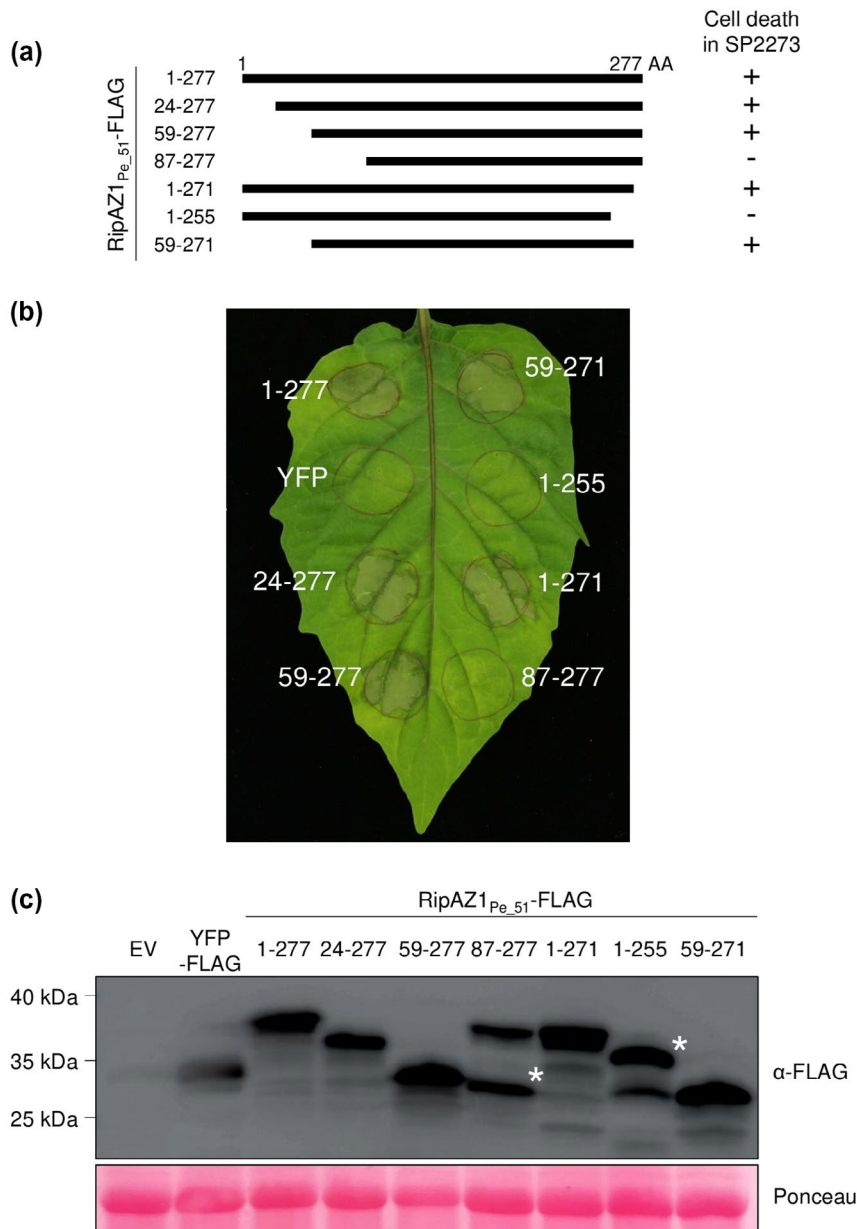


FIGURE 5 Analysis of truncated RipAZ1 defines the minimal region sufficient for cell death-inducing activity. Schematics (a), cell death responses in SP2273 (b), and western blot analysis in *Nicotiana benthamiana* (c) of truncated variants of RipAZ1_{Pe_51}-FLAG. (a) The N- or C-terminally truncated variants of RipAZ1_{Pe_51} were based on the predicted secondary structure (Figure S10). Numbers indicate amino acids. Variants inducing cell death in SP2273 are indicated on the right panel with "+". (b) The photograph was taken at 2 days postinfiltration. White circles indicate the infected leaf area showing cell death. (c) Empty vector (EV; pICH86988) and YFP-FLAG were used as controls. Proteins were immunoblotted with anti-FLAG antibody. Leaf tissue was harvested at 2 days postinfiltration. The protein bands with expected molecular weight are indicated with white asterisks. Ponceau staining shows equal loading of proteins

disordered region (first to 42nd amino acids) and the first α -helix αA (Figure S10), is not required for the recognition. As the N-terminus is predicted to be a disordered region, it may contain a type III secretion signal similar to many other T3Es (Guttman & Greenberg, 2001; Mudgett & Staskawicz, 1999). Further C-terminal truncation from RipAZ1⁵⁹⁻²⁷¹ led to the loss of its recognition. Based on our survey and result with RipAZ1_{To_1}, RipAZ1 natural variants that may have lost avirulence due to frameshift mutations were found (Table S2 and Figure 4). This may be an indication of the evolutionary pressure for *R. solanacearum* to evade recognition of RipAZ1 in nature. Interestingly, C-terminal extension (279th to 284th amino acids) of RipAZ1 natural variants in phylotype IV strains maintained the cell death-inducing activity (Figure 4b). Furthermore, based on our survey of RipAZ1 polymorphisms in multiple *R. solanacearum* strains (Figure 4a), many nonsynonymous single nucleotide polymorphisms (SNPs) found in the minimal region sufficient

for avirulence did not affect RipAZ1 avirulence. Despite our efforts to predict biochemical function of RipAZ1 based on the secondary structure, we were unable to obtain a meaningful result. To get insights into RipAZ1 biochemical function, it will be important to investigate its tertiary structure in future.

The *Arabidopsis* NLR protein RRS1 localizes exclusively in the nucleus when PopP2 is present (Deslandes et al., 2003). Subsequently, PopP2 acetylates and reconfigures RRS1 in the plant cell nucleus and activates RPS4-dependent immunity (Guo et al., 2020; Le Roux et al., 2015; Sarris et al., 2015). Interestingly, it was also shown that the *Arabidopsis* cysteine protease RD19 (Response to Dehydration 19), which is required for RRS1-dependent immunity, relocalizes to the plant nucleus in the presence of PopP2 (Bernoux et al., 2008). In contrast to PopP2, the forced localization of RipAZ1 to the cytoplasm did not result in loss of avirulence function. Based on this observation, it is reasonable to hypothesize that the corresponding R protein

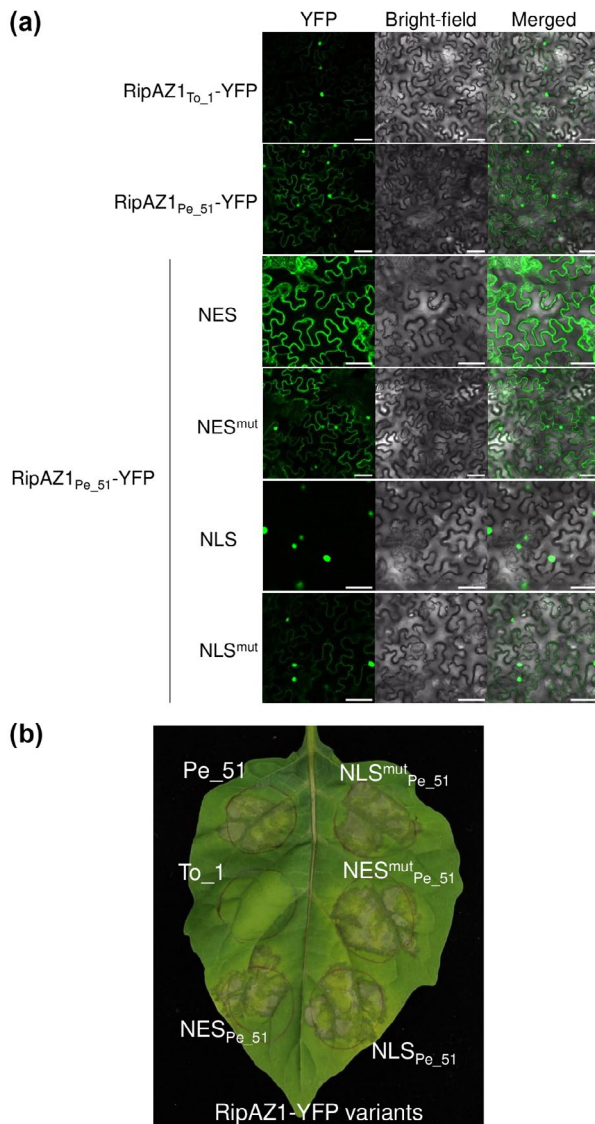


FIGURE 6 RipAZ1-YFP localizes in the nucleus and cytoplasm when transiently expressed in *Nicotiana benthamiana* leaf epidermal cells. Subcellular localization in *N. benthamiana* (a) and cell death responses in SP2273 (b) of RipAZ1-YFP variants when transiently expressed using agroinfiltration. (a) YFP signals were observed at 2 days postinfiltration. Scale bar = 50 μ m. (b) The photograph was taken at 2 days postinfiltration

capable of recognizing RipAZ1 functions in the cytoplasm and nucleus. Alternatively, a guard/decoy protein targeted by RipAZ1 could relocate to the subcellular compartment where the corresponding R protein is present. For example, the 50 kDa helicase (p50) domain of tobacco mosaic virus interacts with N receptor-interacting protein NRIP1 and induces its localization to the cytoplasm and nucleus to activate N protein-dependent immunity (Caplan et al., 2008). Previously, many pathogen effectors were shown to localize to both nucleus and cytoplasm in plant cells (Choi et al., 2017). In addition to the aforementioned PopP2, *P. syringae* T3E AvrRps4 localized in plant cell nucleus and cytoplasm is recognized by RPS4/RRS1 paired NLR proteins. Interestingly, AvrRps4 induces cell compartment-specific defence responses (Heidrich et al., 2011). However, it seems

unlikely that a similar mechanism exists for RipAZ1 because forced localization in the nucleus or cytoplasm did not affect cell death-inducing activity. Taken together, identification of the corresponding R protein and/or the direct target would significantly help elucidate the molecular basis of RipAZ1-triggered defence activation.

Identification of avirulence proteins secreted by pathogens is an important step towards effector-assisted molecular breeding for enhanced disease resistance (Jayaraman et al., 2016; Vleeshouwers & Oliver, 2014). Our finding that RipAZ1 functions as an avirulence determinant of the *R. solanacearum*-*S. americanum* interaction suggests a possibility of identifying a novel bacterial wilt resistance gene using RipAZ1-induced cell death as a proxy for a disease resistance phenotype. Recognition of avirulence effectors by corresponding NLR proteins generally results in the activation of strong defence responses and restricts pathogen proliferation. However, pathogens often overcome the plant defence through modification of the effector repertoire. A bacterial spot pathogen *Xanthomonas euvesicatoria* T3E protein AvrBs2 is known to be highly conserved because it is required for full pathogen virulence (Gassmann et al., 2000; Kearney & Staskawicz, 1990). Hence, it would be necessary to test if RipAZ1 is required for full virulence of *R. solanacearum*. Of note, our transient assay results in *N. benthamiana* suggest that RipAZ1 could modulate host defence responses (Figure S9). Hence, it is plausible that RipAZ1 contributes to the full virulence of *R. solanacearum*. If RipAZ1 is essential for pathogen virulence, the corresponding R gene may be used to develop durable disease resistance in the future.

Pathogens are under constant evolutionary pressure to evade recognition. As a result, loss-of-function mutations are often identified in avirulence effectors (Gassmann et al., 2000; Jones & Dangl, 2006). Therefore, introducing multiple NLRs and pattern-recognition receptors (PRRs) with distinct ligand recognition specificities in a crop cultivar is desirable to achieve durable disease resistance. R gene pyramiding would be particularly ideal for developing durable disease resistance to *R. solanacearum* due to its highly polymorphic T3E repertoires (Fukuoka et al., 2015). The *Arabidopsis* PRR elongation factor-Tu (EF-Tu) receptor (EFR) detects bacterial EF-Tu and activates antibacterial immunity (Jones & Dangl, 2006; Lacombe et al., 2010). Significantly, the interfamily transfer of EFR has resulted in enhanced bacterial wilt resistance in several plant species, including *Solanum lycopersicum*, *Solanum commersonii*, *N. benthamiana*, and *Medicago truncatula* (Boschi et al., 2017; Lacombe et al., 2010; Pfeilmeier et al., 2019). In addition to the aforementioned NLRs such as RPS4/RRS, Roq1, and Ptr1, identification of an additional R protein that recognizes RipAZ1 would be helpful in developing durable bacterial wilt resistance. If successfully identified in the future, deployment of the RipAZ1-recognizing R gene would be highly valuable particularly with Roq1 when introduced in a crop species because the two R genes are predicted to confer resistance to more than 80% of *R. solanacearum* strains based on our survey results (Table S2) and the RalstoT3E database (Peeters et al., 2013). However, we expect that the *S. americanum* R gene recognizing RipAZ1 alone may also be used to develop bacterial wilt-resistant crops. In particular, the RipAZ1-recognizing R gene could be most useful in conferring bacterial wilt

resistance against *R. solanacearum* phylotype IV where more than 85% of strains seem to carry functional *ripAZ1* (Table S2). Moreover, the RipAZ1 recognition property might be particularly useful for developing a bacterial wilt-resistant eggplant cultivar. Sabbagh et al. (2019) have reported that all the strains isolated from eggplant ($n = 9$) carry *ripAZ1*. Consistently, 10 out of 11 strains isolated from eggplant in our survey (Table S2) seem to carry functional *ripAZ1*. Witek et al. (2016) have shown that transgenic potato plants expressing the *S. americanum* NLR *Rpi-amr3* are resistant to *P. infestans*. Because *R. solanacearum* is one of the major pathogens of potato, identification of the *S. americanum* *R* gene recognizing RipAZ1 may help to develop a potato variety that is resistant to both *P. infestans* and *R. solanacearum* in the future.

4 | EXPERIMENTAL PROCEDURES

4.1 | Plant materials and growth conditions

S. americanum accessions used in this study were obtained from The Sainsbury Laboratory (Norwich, UK) and are indicated in Table S1. *S. americanum* seeds were placed on a wet tissue and incubated at 28/18 °C for 16 /8 hr, respectively, with 70% humidity for 1 week for germination. Seedlings were then transferred to individual cell trays and grown for 4 weeks in a controlled room at 24 °C with 16 hr of light a day. *N. benthamiana* seeds were sown, germinated, and grown in individual pots for 4–6 weeks in the controlled growth room with the same conditions.

4.2 | Bacterial strains and culture conditions

The bacterial strains used in this study are indicated in Table 1. Cloning of constructs was carried out in *Escherichia coli* DH5 α . Transient expression assay for macroscopic cell death, western blot, and confocal microscopy was carried out using *Agrobacterium tumefaciens* AGL1. Soil-drenching infection was achieved using *R. solanacearum* strains. *E. coli* and *A. tumefaciens* strains were grown in liquid Luria medium supplemented with appropriate antibiotics for 24 hr at 37 and 28 °C, respectively. *R. solanacearum* strains were grown on peptone broth medium (1% Bacto peptone, 0.1% yeast extract, 0.1% casamino acid) for genomic DNA extraction and natural transformation, or BG complete medium (peptone broth medium supplemented with 0.005% triphenyl tetrazolium chloride [TTC], 1.5% Bacto agar, and 0.5% glucose) for soil-drenching infection, with appropriate antibiotics for 48 hr at 28 °C (Boucher et al., 1985).

4.3 | Soil-drenching infection

R. solanacearum cells were scraped off the growth medium plates with 10 mM MgCl₂ and collected in conical tubes. The bacterial suspension was diluted to OD₆₀₀ 0.5 (approximately 5×10^8 cfu/ml)

with 10 mM MgCl₂. Roots were artificially wounded with a scalpel and the soil in each pot was drenched with 15 ml of the diluted bacterial suspension. Plants were then incubated for 10–20 days in the controlled growth room for observation of disease symptoms.

4.4 | Survival analysis for disease quantification

Plants were infected with *R. solanacearum* strains using the soil-drenching infection assay. A total of 24 plants were tested for each strain. The number of surviving plants was counted on a daily basis. Plants with complete wilting were considered dead (Lonjon et al., 2017). The percentage of survival was plotted using the Kaplan–Meier survival analysis with log-rank (Mantel–Cox) test. *p* values smaller than 0.05 indicate significant differences among survival curves of the tested strains. Graphs and statistical analyses were generated with Prism v. 8.4.3 (GraphPad Software Inc.).

4.5 | Agrobacterium-mediated transient transformation

Binary constructs (pICH86988 and its derivatives; Table 1) were introduced into *A. tumefaciens* AGL1 by electroporation and the resulting transformants were selected on low salt Luria (L) agar medium containing kanamycin (50 μ g/ml). Each *A. tumefaciens* AGL1 transformant was cultured in 3 ml of L medium supplemented with kanamycin (50 μ g/ml) for 2 days at 28 °C with shaking (200 rpm). The cultured cells harbouring pICH86988 or its derivative were harvested by centrifugation and resuspended in infiltration buffer (10 mM MgCl₂, 10 mM MES adjusted to pH 5.6 with KOH). The optical density of the suspension was adjusted to OD₆₀₀ 0.4. The bacterial suspension was infiltrated into the abaxial side of 4-week-old leaves using a blunt-end needless syringe. Macroscopic cell death was observed and photographed at 2–4 days postinfiltration. For protein expression analysis, *A. tumefaciens* AGL1 harbouring P19, a viral silencing suppressor, was coexpressed with all samples after its optical density was adjusted to OD₆₀₀ 0.1.

4.6 | Conductivity measurement

Following *Agrobacterium*-mediated transient transformation, three leaf discs of 9 mm diameter were harvested, transferred to 2 ml of fresh water, and incubated at room temperature for 2 hr with mild shaking (50–100 rpm). The conductivities of three technical replicates per experiment were measured right after infiltration (0 hpi) and every 24 hr until 48 or 72 hpi with a LAQUAtwin EC-33 conductivity meter (Horiba). The conductivity measurements of biological repeats were pooled and the average value is shown. Two-tailed Student's *t* test was conducted to provide groups showing statistically significant differences ($p < .05$).

4.7 | Preparation and natural transformation of *R. solanacearum* competent cells

The protocol of Perrier et al. (2018) was followed with minor modifications. A single colony of *R. solanacearum* was inoculated into 20 ml of one-quarter strength M63 minimal medium (15 mM ammonium sulphate, 1.8 μ M iron(II) sulphate, 100 mM monopotassium phosphate, and 1 mM magnesium sulphate adjusted to pH 7 with KOH) supplemented with 2% glycerol (Miller, 1992) and incubated overnight at 28 °C with shaking (200 rpm). From 500 ng to 200 μ g of plasmid DNA for integration into the bacterial genome was prepared and linearized using *Sfi*I, which does not cut between the two homologous recombination sequences. The linearized plasmid constructs were purified using a Sepharose 4B column. Bacterial cells were harvested by centrifugation at 6,000 \times g for 5 min when the culture reached OD₆₀₀ 0.4 to 0.6. The volume of the cells to be collected was proportional to the amount of the plasmid material (1:10 vol/wt). The purified DNA was added to the bacterial cells and gently mixed with a pipette. The mixture was spotted on a peptone broth agar medium supplemented with 1.5% Bacto agar and incubated for 2 days at 28 °C. Grown cells were collected using a sterile spreader and transferred to a new peptone broth agar medium supplemented with appropriate antibiotics. The agar medium was incubated at 28 °C for 2–3 days. The selected colonies were streaked on a new BG complete medium supplemented with the antibiotics and colony morphology was confirmed using TTC for its virulence.

4.8 | pRCgg plasmid vector construction

The pRC (the *Ralstonia* chromosome) vector series is a powerful tool developed by Monteiro et al. (2012) that can integrate a gene fragment of interest (GOI) cloned using the Gateway cloning system into an *R. solanacearum* chromosomal site through a double recombination event. Here, pRCgg plasmid vectors were generated to transform GOIs into *R. solanacearum* genomes using the Golden Gate cloning system. pICH41021 was used as a backbone plasmid for pRCgg (Table 1). The *lacZ* cassette was amplified using standard PCR conditions to contain *Bam*HI and *Eco*RI recognition sequences at 5' and 3' ends, respectively, followed by *Bsa*I recognition sequences at both ends. *Bam*HI and *Eco*RI sites within the cassette were then removed by site-directed mutagenesis. The 5'-*Bam*HI-*Bsa*I-*lacZ*-*Bsa*I-*Eco*RI-3' fragment was ligated into pICH41021 with conventional restriction enzyme cloning to make the pRCgg plasmid (Table 1 and Figure S3A).

Next, GMI-1 and GMI-2, which are conserved genomic regions used for homologous recombination, transcriptional terminators (*Tfd* and *Tt7* terminators), and kanamycin resistance cassette were separately amplified from pRCK (Monteiro et al., 2012) and prepared as Golden Gate module constructs in pICH41021, flanked by *Bsa*I recognition sites (Engler et al., 2008). Two *Bsa*I sites within GMI-2 were removed by site-directed mutagenesis for further vector construction. To replace the Gateway cassette in pRC vector, another

lacZ cassette amplified from pICH86988 (Weber et al., 2011) was prepared as a pICH41021 module construct, also flanked by *Bsa*I recognition sites. Six modules (GMI-1, *Tfd* terminators, kanamycin resistance cassette, *lacZ* cassette for Golden Gate cloning, *Tt7* terminator, and GMI-2) were then assembled in the pRCgg plasmid (Figure S3a), converting pRCK to pRCgg (Table 1 and Figure S3b).

4.9 | Plasmid construction

Effector constructs were cloned using the Golden Gate cloning system as explained by Engler et al. (2008). Genomic DNA of *R. solanacearum* Pe₂₆, Pe₅₁, Pe₅₇, To₁, SL3022, and KACC10722 was extracted using the Wizard Genomic DNA Purification Kit (Promega) following the manufacturer's instructions to be used as a PCR template. Gene fragments for some effectors (*ripAZ1*, *ripTAL*, *ripY*, and *RS_T3E_Hyp6*) were amplified from the *R. solanacearum* genomic DNA using standard PCR conditions to have *Bsa*I recognition sites at the 5' and 3' ends. To construct RipAZ1 truncated variants (Table 1), ATG was additionally included following the *Bsa*I recognition site in forward primers. To construct C-terminal epitope tag YFP-NES, YFP-NLS, YFP-NES^{mut}, and YFP-NLS^{mut} modules, DNA fragments encoding the four aforementioned epitope tags were amplified from pICH86988-YFP using standard PCR conditions to have NES, NLS, NES^{mut}, or NLS^{mut} at the 3' end (NES: LALKLAGLDI; NES^{mut}: LALKAAGADA; NLS: PKKKRKYVGG; NLS^{mut}: PKTKRKYVGG) (Heidrich et al., 2011; Wen et al., 1995). All the amplified DNA fragments were cloned in *Sma*I-treated pICH41021 shuttle vector (Table 1). Gene fragments for other effectors (*ripBA*, *ripG1*, *ripAX1*, *ripB*, *ripG6*, *ripA3*, *ripD*, and *ripJ*) were synthesized with their codons optimized for synthesis (codon-optimized sequences are available upon request) and attached with *Bsa*I recognition sites at the 5' and 3' ends by Integrated DNA Technologies (IDT). The synthesized gene fragments were cloned in pICH41021 using *Sma*I (Table 1) by IDT. DNA sequences of these constructs were verified by sequencing using M13F and M13R primers performed by Solgent. Gene modules cloned in pICH41021 were assembled using *Bsa*I into pICH86988 or pRCKgg with an appropriate promoter and/or appropriate C-terminal epitope tags (Table 1 and Figure S3b). Assembled constructs were selected with appropriate antibiotics of the destination vectors and screened with blue-white selection using 15 μ l of 100 mM IPTG and 800 μ g X-gal. The constructs were finally verified by restriction enzyme digestion, followed by visualization in agarose gel electrophoresis.

To obtain the *ripAZ1* knockout plasmid following Wu et al. (2018), 1,000 bp of 5' sequence of the *ripAZ1* ORF and 972 bp consisting of 78 bp of *ripAZ1* ORF sequence from its 3' end and 894 bp of its 3' sequence was amplified from *R. solanacearum* Pe₂₆ genomic DNA to have *Bsa*I at both 5' and 3' ends and cloned in pICH41021 to be homologous recombination fragments. A Spec^R cassette amplified from pCR8 (Invitrogen) flanked by *Bsa*I at both ends was also cloned in pICH41021. These modules were assembled using *Bsa*I into pRCgg plasmid (Table 1 and Figure S3a) and selected with ampicillin and spectinomycin. The

assembled pRCgg- Δ ripAZ1 (Table 1) was verified by restriction enzyme digestion, followed by visualization in agarose gel electrophoresis.

4.10 | Total protein extraction from plant tissues and western blot

Plant tissues were harvested at 2–3 dpi and immediately snap-frozen in liquid nitrogen. The harvested samples were ground and mixed with 250 μ l of 5 \times SDS sample buffer (250 mM Tris-HCl adjusted to pH 6.8, 10% sodium dodecyl sulphate [SDS], 0.1% [wt/vol] bromophenol blue, and 40% glycerol, supplemented with 50 mM dithiothreitol before use). The mixture was boiled at 96 $^{\circ}$ C for 10 min, vortexed vigorously, and centrifuged at 15,000 \times g for 1 min. Fifteen microlitres of the supernatant was used for SDS-polyacrylamide gel electrophoresis (PAGE) to separate proteins. Samples were run on an SDS-polyacrylamide gel with 120 V for 80 min, electroblotted onto a PVDF membrane with 300 mA for 120 min and probed with anti-FLAG (Sigma-Aldrich) and anti-mouse antibody conjugated to horseradish peroxidase (HRP) (Sigma-Aldrich) or with HRP-conjugated anti-GFP (Santa Cruz). Visualization was achieved using SuperSignal West Pico and Femto substrate (Thermo Scientific) in ImageQuant LAS 500 chemiluminescence CCD camera (GE Healthcare). Lastly, the membrane was stained with Ponceau S (Sigma-Aldrich) for 10 min to visualize total protein loading.

4.11 | Measurement of ROS production

Leaf discs of 5 mm diameter were collected from *N. benthamiana* leaf tissue expressing RipAZ1_{Pe_26}, RipAZ1_{To_1}, or YFP and were floated on 150 μ l of deionized water overnight. The water was replaced with 100 μ l of solution containing 100 μ M luminol (Sigma-Aldrich), 2 μ g of peroxidase from horseradish (Sigma-Aldrich), and 50 nM of flg22 (Peptron). Luminescence was measured for 75 min using GloMax 96 microplate luminometer (Promega) and data were recorded as total counts of relative light unit (RLU).

4.12 | Quantitative reverse transcription PCR

Two leaf discs of 8 mm diameter were collected from *N. benthamiana* leaf tissue expressing RipAZ1_{Pe_26}, RipAZ1_{To_1}, or YFP at 1 day postinfiltration and floated on deionized water overnight. At 2 days postinfiltration, the leaf discs were treated with 100 nM flg22 or water for 1 hr and frozen for RNA extraction. Total RNA was extracted using TRI reagent (MRC) and treated with DNase I (Sigma-Aldrich). RNA (2.5 μ g) was used to synthesize cDNA using a Maxima first-strand cDNA synthesis kit (Thermo Scientific). For quantitative PCR, cDNA was combined with GoTaq qPCR master mix (Promega) and PCR was performed in triplicate with a CFX connect real-time system (Bio-Rad). Expression was normalized to the reference gene *NbEF1 α* . Primers for genes used here are as follows:

NbEF1 α , 5'-AGGTCCAGTATGCCTGGGTGCTTGAC-3' and 5'-AAG AATTCACAGGGACAGTTCCAATACCAC-3'; *NbCYP71D20*, 5'-AAGG TCCACCGCACCATGTCCTTAGAG-3' and 5'-AAGAATTCCTTGCC CCTTGAGTACTTGC-3'; *NbACRE31*, 5'-AAGGTCCCGTCTTCGTC GGATCTTCG-3' and 5'-AAGAATTCGGCCATCGTGATCTTGGTC-3' (Segonzac et al., 2011).

4.13 | Protein secondary structure prediction

The secondary structure of RipAZ1 was modelled using various programs, LRRfinder (Offord et al., 2010), PSIPRED (Buchan & Jones, 2019; Jones, 1999), InterProScan (Jones et al., 2014), and a plug-in EMBOSS Garnier (Rice et al., 2000) for Geneious v. 11.1.5 (Biomatters, Auckland, New Zealand).

4.14 | Confocal microscopy

A. tumefaciens AGL1 carrying C-terminal YFP-tagged *ripAZ1* with or without various localization signals was infiltrated in *N. benthamiana* leaves. Leaf discs were taken at 2 days postinfiltration from the infiltrated area and mounted in water for confocal laser scanning microscopy. YFP signals were monitored in a confocal laser scanning microscope (FV3000, Olympus). The signals were excited with a 488 nm ray line of the argon laser and detected in a confocal channel in the 500–600 nm emission range, applied with a photomultiplier voltage 483 V. Images were obtained using the manufacturer's software Fluoview FV315-SW (Olympus).

ACKNOWLEDGEMENTS

We thank Dr Heejung Cho and Dr Young Kee Lee for *R. solanacearum* strains and Dr Jay Jayaraman for critical reading of the manuscript. This work was supported by a grant from the Next-Generation BioGreen 21 Program (Plant Molecular Breeding Center no. PJ01317501), the Rural Development Administration and National Research Foundation of Korea (NRF) grants funded by the Korea government (MSIT) (NRF-2019R1A2C2084705 & 2018R1A5A1023599 (SRC)), Republic of Korea. C.S. was supported by the Creative-Pioneering Researchers Program through Seoul National University. M.V.'s research was funded by the research grants (PID2019-108595RB-I00 and SEV/2015/0533) from the Spanish Government and the CERCA Program from the Catalan Government (Generalitat de Catalunya). The authors declare no conflicts of interest.

DATA AVAILABILITY STATEMENT

The data that support the findings of this study are available from the corresponding author upon reasonable request.

ORCID

Marc Valls  <https://orcid.org/0000-0003-2312-0091>

Kee Hoon Sohn  <https://orcid.org/0000-0002-9021-8649>

REFERENCES

- Arlat, M., Van Gijsegem, F., Huet, J.C., Pernollet, J.C. & Boucher, C.A. (1994) PopA1, a protein which induces a hypersensitivity-like response on specific *Petunia* genotypes, is secreted via the Hrp pathway of *Pseudomonas solanacearum*. *EMBO Journal*, **13**, 543–553.
- Asai, S., Furzer, O.J., Cevik, V., Kim, D.S., Ishaque, N., Goritschnig, S. et al. (2018) A downy mildew effector evades recognition by polymorphism of expression and subcellular localization. *Nature Communications*, **9**, 5192.
- Baggs, E., Dagdas, G. & Krasileva, K.V. (2017) NLR diversity, helpers and integrated domains: making sense of the NLR IDentity. *Current Opinion in Plant Biology*, **38**, 59–67.
- Belbahri, L., Boucher, C., Candresse, T., Nicole, M., Ricci, P. & Keller, H. (2001) A local accumulation of the *Ralstonia solanacearum* PopA protein in transgenic tobacco renders a compatible plant-pathogen interaction incompatible. *The Plant Journal*, **28**, 419–430.
- Bergelson, J., Kreitman, M., Stahl, E.A. & Tian, D. (2001) Evolutionary dynamics of plant R-genes. *Science*, **292**, 2281–2285.
- Bernoux, M., Timmers, T., Jauneau, A., Briere, C., De Wit, P.J., Marco, Y. et al. (2008) RD19, an *Arabidopsis* cysteine protease required for RRS1-R-mediated resistance, is relocalized to the nucleus by the *Ralstonia solanacearum* PopP2 effector. *The Plant Cell*, **20**, 2252–2264.
- Bos, J.I., Kanneganti, T.D., Young, C., Cakir, C., Huitema, E., Win, J. et al. (2006) The C-terminal half of *Phytophthora infestans* RXLR effector AVR3a is sufficient to trigger R3a-mediated hypersensitivity and suppress INF1-induced cell death in *Nicotiana benthamiana*. *The Plant Journal*, **48**, 165–176.
- Boschi, F., Schwartzman, C., Murchio, S., Ferreira, V., Siri, M.I., Galvan, G.A. et al. (2017) Enhanced bacterial wilt resistance in potato through expression of *Arabidopsis* EFR and introgression of quantitative resistance from *Solanum commersonii*. *Frontiers in Plant Science*, **8**, 1642.
- Boucher, C.A., Barberis, P.A. & Demery, D.A. (1985) Transposon mutagenesis of *Pseudomonas solanacearum*: isolation of Tn5-induced avirulent mutants. *Microbiology*, **131**, 2449–2457.
- Buchan, D.W.A. & Jones, D.T. (2019) The PSIPRED protein analysis workbench: 20 years on. *Nucleic Acids Research*, **47**, W402–W407.
- Caplan, J.L., Mamillapalli, P., Burch-Smith, T.M., Czymmek, K. & Dinesh-Kumar, S.P. (2008) Chloroplastic protein NRIP1 mediates innate immune receptor recognition of a viral effector. *Cell*, **132**, 449–462.
- Catanzariti, A.M., Dodds, P.N., Ve, T., Kobe, B., Ellis, J.G. & Staskawicz, B.J. (2010) The AvrM effector from flax rust has a structured C-terminal domain and interacts directly with the M resistance protein. *Molecular Plant-Microbe Interactions*, **23**, 49–57.
- Cesari, S. (2018) Multiple strategies for pathogen perception by plant immune receptors. *New Phytologist*, **219**, 17–24.
- Chen, L., Dahal, A., Zhang, Y., Rokunuzzaman, M., Kiba, A., Hikichi, Y. et al. (2018) Involvement of avirulence genes *avrA* and *popP1* of Japanese *Ralstonia solanacearum* strains in the pathogenicity to tobacco. *Physiological and Molecular Plant Pathology*, **102**, 154–162.
- Choi, S., Jayaraman, J., Segonzac, C., Park, H.J., Park, H., Han, S.W. et al. (2017) *Pseudomonas syringae* pv. *actinidiae* type III effectors localized at multiple cellular compartments activate or suppress innate immune responses in *Nicotiana benthamiana*. *Frontiers in Plant Science*, **8**, 2157.
- Clarke, C.R., Studholme, D.J., Hayes, B., Runde, B., Weisberg, A., Cai, R. et al. (2015) Genome-enabled phylogeographic investigation of the quarantine pathogen *Ralstonia solanacearum* race 3 biovar 2 and screening for sources of resistance against its core effectors. *Phytopathology*, **105**, 597–607.
- Coll, N.S. & Valls, M. (2013) Current knowledge on the *Ralstonia solanacearum* type III secretion system. *Microbial Biotechnology*, **6**, 614–620.
- Denny, T. (2007) Plant pathogenic *Ralstonia* species. In: Gnanamanickam, S.S. ed. *Plant-associated Bacteria*. Dordrecht: Springer, pp. 573–644.
- Deslandes, L., Olivier, J., Peeters, N., Feng, D.X., Khounloham, M., Boucher, C. et al. (2003) Physical interaction between RRS1-R, a protein conferring resistance to bacterial wilt, and PopP2, a type III effector targeted to the plant nucleus. *Proceedings of the National Academy of Sciences of the United States of America*, **100**, 8024–8029.
- Deslandes, L., Olivier, J., Theulieres, F., Hirsch, J., Feng, D.X., Bittner-Eddy, P. et al. (2003) Resistance to *Ralstonia solanacearum* in *Arabidopsis thaliana* is conferred by the recessive RRS1-R gene, a member of a novel family of resistance genes. *Proceedings of the National Academy of Sciences of the United States of America*, **99**, 2404–2409.
- Dodds, P.N., Lawrence, G.J., Catanzariti, A.M., Teh, T., Wang, C.I., Ayliffe, M.A. et al. (2006) Direct protein interaction underlies gene-for-gene specificity and coevolution of the flax resistance genes and flax rust avirulence genes. *Proceedings of the National Academy of Sciences of the United States of America*, **103**, 8888–8893.
- Edmonds, J.M. & Chweya, J.A. (1997) *Black Nightshades: Solanum nigrum L. and Related Species*. Institute of Plant Genetics and Crop Plant Research, Gatersleben/International Plant Genetic Resources Institute. Rome, Italy: Bioversity International.
- Engler, C., Kandzia, R. & Marillonnet, S. (2008) A one pot, one step, precision cloning method with high throughput capability. *PLoS One*, **3**, e3647.
- Fegan, M. & Prior, P. (2005). How complex is the *Ralstonia solanacearum* species complex? In: Allen, C., Prior, P. & Hayward, A.C. (Eds.). *Bacterial wilt disease and the Ralstonia solanacearum species complex*. St Paul, MN: APS Press, pp. 449–461.
- Fukuoka, S., Saka, N., Mizukami, Y., Koga, H., Yamanouchi, U., Yoshioka, Y. et al. (2015) Gene pyramiding enhances durable blast disease resistance in rice. *Scientific Reports*, **5**, 7773.
- Ganapathi, A. & Rao, G.R. (1987) Phylogenetic relationships in the evolution of *Solanum scabrum*. *Genome*, **29**, 639–642.
- Gassmann, W., Dahlbeck, D., Chesnokova, O., Minsavage, G.V., Jones, J.B. & Staskawicz, B.J. (2000) Molecular evolution of virulence in natural field strains of *Xanthomonas campestris* pv. *vesicatoria*. *Journal of Bacteriology*, **182**, 7053–7059.
- Genin, S. & Denny, T.P. (2012) Pathogenomics of the *Ralstonia solanacearum* species complex. *Annual Review of Phytopathology*, **50**, 67–89.
- Guo, H., Ahn, H.K., Sklenar, J., Huang, J., Ma, Y., Ding, P. et al. (2020) Phosphorylation-regulated activation of the *Arabidopsis* RRS1-R/RPS4 immune receptor complex reveals two distinct effector recognition mechanisms. *Cell Host & Microbe*, **27**, 769–781.
- Guttman, D.S. & Greenberg, J.T. (2001) Functional analysis of the type III effectors AvrRpt2 and AvrRpm1 of *Pseudomonas syringae* with the use of a single-copy genomic integration system. *Molecular Plant-Microbe Interactions*, **14**, 145–155.
- Heidrich, K., Wirthmueller, L., Tasset, C., Pouzet, C., Deslandes, L. & Parker, J.E. (2011) *Arabidopsis* EDS1 connects pathogen effector recognition to cell compartment-specific immune responses. *Science*, **334**, 1401–1404.
- Jayaraman, J., Segonzac, C., Cho, H., Jung, G. & Sohn, K.H. (2016) Effector-assisted breeding for bacterial wilt resistance in horticultural crops. *Horticulture, Environment, and Biotechnology*, **57**, 415–423.
- Jeon, H., Kim, W., Kim, B., Lee, S., Jayaraman, J., Jung, G. et al. (2020) *Ralstonia solanacearum* type III effectors with predicted nuclear localization signal localize to various cell compartments and modulate immune responses in *Nicotiana* spp. *Plant Pathology Journal*, **36**, 43–53.
- Jones, D.T. (1999) Protein secondary structure prediction based on position-specific scoring matrices. *Journal of Molecular Biology*, **292**, 195–202.
- Jones, J.D. & Dangl, J.L. (2006) The plant immune system. *Nature*, **444**, 323–329.

- Jones, J.D., Vance, R.E. & Dangl, J.L. (2016) Intracellular innate immune surveillance devices in plants and animals. *Science*, 354, aaf6395.
- Jones, P., Binns, D., Chang, H.Y., Fraser, M., Li, W., McAnulla, C. et al. (2014) InterProScan 5: genome-scale protein function classification. *Bioinformatics*, 30, 1236–1240.
- Jwa, N.S. & Hwang, B.K. (2017) Convergent evolution of pathogen effectors toward reactive oxygen species signaling networks in plants. *Frontiers in Plant Science*, 8, 1687.
- Kearney, B. & Staskawicz, B.J. (1990) Widespread distribution and fitness contribution of *Xanthomonas campestris* avirulence gene *avrBs2*. *Nature*, 346, 385–386.
- Kearse, M., Moir, R., Wilson, A., Stones-Havas, S., Cheung, M., Sturrock, S. et al. (2012) Geneious Basic: an integrated and extendable desktop software platform for the organization and analysis of sequence data. *Bioinformatics*, 28, 1647–1649.
- Lacombe, S., Rougon-Cardoso, A., Sherwood, E., Peeters, N., Dahlbeck, D., Van Esse, H.P. et al. (2010) Interfamily transfer of a plant pattern-recognition receptor confers broad-spectrum bacterial resistance. *Nature Biotechnology*, 28, 365–369.
- Lavie, M., Shillington, E., Eguiluz, C., Grimsley, N. & Boucher, C. (2002) PopP1, a new member of the YopJ/AvrRxv family of type III effector proteins, acts as a host-specificity factor and modulates aggressiveness of *Ralstonia solanacearum*. *Molecular Plant-Microbe Interactions*, 15, 1058–1068.
- Le Roux, C., Huet, G., Jauneau, A., Camborde, L., Tremousaygue, D., Kraut, A. et al. (2015) A receptor pair with an integrated decoy converts pathogen disabling of transcription factors to immunity. *Cell*, 161, 1074–1088.
- Lonjon, F., Lohou, D., Cazale, A.C., Buttner, D., Ribeiro, B.G., Pianne, C. et al. (2017) HpaB-dependent secretion of type III effectors in the plant pathogens *Ralstonia solanacearum* and *Xanthomonas campestris* pv. *vesicatoria*. *Scientific Reports*, 7, 4879.
- Ma, W., Dong, F.F., Stavrinides, J. & Guttman, D.S. (2006) Type III effector diversification via both pathoadaptation and horizontal transfer in response to a coevolutionary arms race. *PLoS Genetics*, 2, e209.
- Macho, A.P. & Zipfel, C. (2015) Targeting of plant pattern recognition receptor-triggered immunity by bacterial type-III secretion system effectors. *Current Opinion in Microbiology*, 23, 14–22.
- Mazo-Molina, C., Mainiero, S., Hind, S.R., Kraus, C.M., Vachev, M., Maviane-Macia, F. et al. (2019) The *Ptr1* locus of *Solanum lycopersicon* confers resistance to race 1 strains of *Pseudomonas syringae* pv. *tomato* and to *Ralstonia pseudosolanacearum* by recognizing the type III effectors AvrRpt2 and RipBN. *Molecular Plant-Microbe Interactions*, 32, 949–960.
- McCann, H.C. & Guttman, D.S. (2008) Evolution of the type III secretion system and its effectors in plant-microbe interactions. *New Phytologist*, 177, 33–47.
- Miller, J.H. (1992) *A short course in bacterial genetics: a laboratory manual and handbook for Escherichia coli and related bacteria*. Cold Spring Harbor, NY: Cold Spring Harbor Laboratory Press.
- Monteiro, F., Sole, M., Van Dijk, I. & Valls, M. (2012) A chromosomal insertion toolbox for promoter probing, mutant complementation, and pathogenicity studies in *Ralstonia solanacearum*. *Molecular Plant-Microbe Interactions*, 25, 557–568.
- Morel, A., Guinard, J., Lonjon, F., Sujeeun, L., Barberis, P., Genin, S. et al. (2018) The eggplant AG91-25 recognizes the type III-secreted effector RipAX2 to trigger resistance to bacterial wilt (*Ralstonia solanacearum* species complex). *Molecular Plant Pathology*, 19, 2459–2472.
- Mudgett, M.B. & Staskawicz, B.J. (1999) Characterization of the *Pseudomonas syringae* pv. *tomato* AvrRpt2 protein: demonstration of secretion and processing during bacterial pathogenesis. *Molecular Microbiology*, 32, 927–941.
- Mukaihara, T., Tamura, N. & Iwabuchi, M. (2010) Genome-wide identification of a large repertoire of *Ralstonia solanacearum* type III effector proteins by a new functional screen. *Molecular Plant-Microbe Interactions*, 23, 251–262.
- Nakano, M. & Mukaihara, T. (2019) The type III effector RipB from *Ralstonia solanacearum* RS1000 acts as a major avirulence factor in *Nicotiana benthamiana* and other *Nicotiana* species. *Molecular Plant Pathology*, 20, 1237–1251.
- Narusaka, M., Kubo, Y., Hatakeyama, K., Imamura, J., Ezura, H., Nanasato, Y. et al. (2013) Interfamily transfer of dual NB-LRR genes confers resistance to multiple pathogens. *PLoS One*, 8, e55954.
- Narusaka, M., Shirasu, K., Noutoshi, Y., Kubo, Y., Shiraishi, T., Iwabuchi, M. et al. (2009) RRS1 and RPS4 provide a dual resistance-gene system against fungal and bacterial pathogens. *The Plant Journal*, 60, 218–226.
- Occhialini, A., Cunnac, S., Reymond, N., Genin, S. & Boucher, C. (2005) Genome-wide analysis of gene expression in *Ralstonia solanacearum* reveals that the *hrpB* gene acts as a regulatory switch controlling multiple virulence pathways. *Molecular Plant-Microbe Interactions*, 18, 938–949.
- Offord, V., Coffey, T.J. & Werling, D. (2010) LRRfinder: a web application for the identification of leucine-rich repeats and an integrative Toll-like receptor database. *Developmental and Comparative Immunology*, 34, 1035–1041.
- Peeters, N., Carrere, S., Anisimova, M., Plener, L., Cazale, A.C. & Genin, S. (2013) Repertoire, unified nomenclature and evolution of the Type III effector gene set in the *Ralstonia solanacearum* species complex. *BMC Genomics*, 14.
- Perrier, A., Barberis, P. & Genin, S. (2018) Introduction of genetic material in *Ralstonia solanacearum* through natural transformation and conjugation. *Methods in Molecular Biology*, 1734, 201–207.
- Pfeilmeier, S., George, J., Morel, A., Roy, S., Smoker, M., Stransfeld, L. et al. (2019) Expression of the *Arabidopsis thaliana* immune receptor EFR in *Medicago truncatula* reduces infection by a root pathogenic bacterium, but not nitrogen-fixing rhizobial symbiosis. *Plant Biotechnology Journal*, 17, 569–579.
- Poueymiro, M., Cazalé, A.C., François, J.M., Parrou, J.L., Peeters, N. & Genin, S. (2014) A *Ralstonia solanacearum* type III effector directs the production of the plant signal metabolite trehalose-6-phosphate. *mBio*, 5, 02065-14.
- Poueymiro, M., Cunnac, S., Barberis, P., Deslandes, L., Peeters, N., Cazale-Noel, A.C. et al. (2009) Two type III secretion system effectors from *Ralstonia solanacearum* GMI1000 determine host-range specificity on tobacco. *Molecular Plant-Microbe Interactions*, 22, 538–550.
- Prokhorchik, M., Pandey, A., Moon, H., Kim, W., Jeon, H., Jung, G. et al. (2020) Host adaptation and microbial competition drive *Ralstonia solanacearum* phylotype I evolution in the Republic of Korea. *Microbial Genomics*, 6, mgen000461.
- Qi, D. & Innes, R.W. (2013) Recent advances in plant NLR structure, function, localization, and signaling. *Frontiers in Immunology*, 4, 348.
- Racape, J., Belbahri, L., Engelhardt, S., Lacombe, B., Lee, J., Lochman, J. et al. (2005) Ca²⁺-dependent lipid binding and membrane integration of PopA, a harpin-like elicitor of the hypersensitive response in tobacco. *Molecular Microbiology*, 58, 1406–1420.
- Rice, P., Longden, I. & Bleasby, A. (2000) EMBOS: the European molecular biology open software suite. *Trends in Genetics*, 16, 276–277.
- Sabbagh, C.R.R., Carrere, S., Lonjon, F., Vaillau, F., Macho, A.P., Genin, S. et al. (2019) Pangenomic type III effector database of the plant pathogenic *Ralstonia* spp. *PeerJ*, 7, e7346.
- Sang, Y., Wenjia, Y., Zhuang, H., Wei, Y., Derevnina, L., Yu, G. et al. (2020) Intra-strain elicitation and suppression of plant immunity by *Ralstonia solanacearum* type-III effectors in *Nicotiana benthamiana*. *Plant Communications*, 1, 100025.
- Sarkinen, T., Pocza, P., Barboza, G.E., Van Der Weerden, G.M., Baden, M. & Knapp, S. (2018) A revision of the old world black nightshades (Morelloid clade of *Solanum* L. Solanaceae). *PhytoKeys*, 106, 1–223.

- Sarris, P.F., Duxbury, Z., Huh, S.U., Ma, Y., Segonzac, C., Sklenar, J. et al. (2015) A plant immune receptor detects pathogen effectors that target WRKY transcription factors. *Cell*, 161, 1089–1100.
- Schultink, A., Qi, T., Lee, A., Steinbrenner, A.D. & Staskawicz, B. (2017) Roq1 mediates recognition of the *Xanthomonas* and *Pseudomonas* effector proteins XopQ and HopQ1. *The Plant Journal*, 92, 787–795.
- Segonzac, C., Feike, D., Gimenez-Ibanez, S., Hann, D.R., Zipfel, C. & Rathjen, J.P. (2011) Hierarchy and roles of pathogen-associated molecular pattern-induced responses in *Nicotiana benthamiana*. *Plant Physiology*, 156, 687–699.
- Segonzac, C., Newman, T.E., Choi, S., Jayaraman, J., Choi, D.S., Jung, G.Y. et al. (2017) A conserved EAR motif is required for avirulence and stability of the *Ralstonia solanacearum* effector PopP2 in planta. *Frontiers in Plant Science*, 8, 1330.
- Sole, M., Popa, C., Mith, O., Sohn, K.H., Jones, J.D., Deslandes, L. et al. (2012) The *avr* gene family encodes a novel class of *Ralstonia solanacearum* type III effectors displaying virulence and avirulence activities. *Molecular Plant-Microbe Interactions*, 25, 941–953.
- Thomas, N.C., Hendrich, C.G., Gill, U.S., Allen, C., Hutton, S.F. & Schultink, A. (2020) The immune receptor Roq1 confers resistance to the bacterial pathogens *Xanthomonas*, *Pseudomonas syringae*, and *Ralstonia* in tomato. *Frontiers in Plant Science*, 11, 463.
- Valls, M., Genin, S. & Boucher, C. (2006) Integrated regulation of the type III secretion system and other virulence determinants in *Ralstonia solanacearum*. *PLoS Pathogens*, 2, e82.
- Vleeshouwers, V.G. & Oliver, R.P. (2014) Effectors as tools in disease resistance breeding against biotrophic, hemibiotrophic, and necrotrophic plant pathogens. *Molecular Plant-Microbe Interactions*, 27, 196–206.
- Weber, E., Engler, C., Gruetzner, R., Werner, S. & Marillonnet, S. (2011) A modular cloning system for standardized assembly of multigene constructs. *PLoS One*, 6, e16765.
- Wen, W., Meinkoth, J.L., Tsien, R.Y. & Taylor, S.S. (1995) Identification of a signal for rapid export of proteins from the nucleus. *Cell*, 82, 463–473.
- Witek, K., Jupe, F., Witek, A.I., Baker, D., Clark, M.D. & Jones, J.D. (2016) Accelerated cloning of a potato late blight-resistance gene using RenSeq and SMRT sequencing. *Nature Biotechnology*, 34, 656–660.
- Wroblewski, T., Caldwell, K.S., Piskurewicz, U., Cavanaugh, K.A., Xu, H., Kozik, A. et al. (2009) Comparative large-scale analysis of interactions between several crop species and the effector repertoires from multiple pathovars of *Pseudomonas* and *Ralstonia*. *Plant Physiology*, 150, 1733–1749.
- Wu, D., Schandry, N. & Lahaye, T. (2018) A modular toolbox for GoldenGate-based plasmid assembly streamlines the generation of *Ralstonia solanacearum* species complex knockout strains and multi-cassette complementation constructs. *Molecular Plant Pathology*, 19, 1511–1522.
- Yang, B., Sugio, A. & White, F.F. (2005) Avoidance of host recognition by alterations in the repetitive and C-terminal regions of AvrXa7, a type III effector of *Xanthomonas oryzae* pv. *oryzae*. *Molecular Plant-Microbe Interactions*, 18, 142–149.
- Yang, B. & White, F.F. (2004) Diverse members of the AvrBs3/PthA family of type III effectors are major virulence determinants in bacterial blight disease of rice. *Molecular Plant-Microbe Interactions*, 17, 1192–1200.
- Zheng, X., Li, X., Wang, B., Cheng, D., Li, Y., Li, W. et al. (2019) A systematic screen of conserved *Ralstonia solanacearum* effectors reveals the role of RipAB, a nuclear-localized effector that suppresses immune responses in potato. *Molecular Plant Pathology*, 20, 547–561.
- Zhuo, T., Wang, X., Chen, Z., Cui, H., Zeng, Y., Chen, Y. et al. (2020) The *Ralstonia solanacearum* effector RipI induces a defence reaction by interacting with the bHLH93 transcription factor in *Nicotiana benthamiana*. *Molecular Plant Pathology*, 21, 999–1004.

SUPPORTING INFORMATION

Additional Supporting Information may be found online in the Supporting Information section.

How to cite this article: Moon H, Pandey A, Yoon H, et al. Identification of RipAZ1 as an avirulence determinant of *Ralstonia solanacearum* in *Solanum americanum*. *Mol Plant Pathol*. 2021;00:1–17. <https://doi.org/10.1111/mpp.13030>